How long does carbon stay in a near-pristine central Amazon forest? An empirical estimate with radiocarbon

Ingrid Chanca[1,2,3,*], Ingeborg Levin[4,†,*], Susan Trumbore[1], Kita Macario[2], Jost Lavric[1,5], Carlos Alberto Quesada[6], Alessandro Carioca de Araújo[7], Cléo Quaresma Dias Júnior[8], Hella van Asperen[1], Samuel Hammer[4], and Carlos A. Sierra[1]

[1]Max Planck Institute for Biogeochemistry, Jena, Germany.
[2]Laboratório de Radiocarbono, Instituto de Física, Universidade Federal Fluminense, Niterói, Brazil.
[3]Now at: Laboratoire des Sciences du Climat et de l'Environnement (LSCE), Orme des Merisiers, Saint-Aubin, France
[4]Institute of Environmental Physics, Heidelberg University, Heidelberg, Germany.
[†]deceased, 10 February 2024
[5]Acoem GmbH, Hallbergmoos, Germany
[6]Instituto Nacional de Pesquisas da Amazônia (INPA), Manaus, Brazil.
[7]Empresa Brasileira de Pesquisa Agropecuária (EMBRAPA) Amazônia Oriental, Belém, Brazil.
[8]Instituto Federal de Educação, Ciência e Tecnologia do Pará, Belém, Brazil.
[*]These authors contributed equally to this work.

Correspondence: Ingrid Chanca (ichanca@bgc-jena.mpg.de)

Abstract. Amazon forests play a significant role in the global C cycle by assimilating large amounts of CO_2 through photosynthesis and storing C largely as biomass and soil organic matter. To evaluate the net budget of C in the Amazon, we must also consider the amplitude and timing of losses of C back to the atmosphere through respiration and biomass burning. One useful timescale metric that integrates such information in terrestrial ecosystems is the transit time of C, defined as the time elapsed between C entering and leaving the ecosystem; transit time is equivalent to the age of C exiting the ecosystem, which occurs mostly through respiration. We estimated the mean transit time of C for a central Amazon forest based on the C age in ecosystem respiration (ER), taking advantage of the large variations in CO_2 in the atmosphere below the forest canopy to estimate the radiocarbon signature of mean ER ($\Delta^{14}C_{ER}$) using Keeling and Miller-Tans mixing models. ~~To~~ We collected air samples to evaluate changes in the isotopic signature of the main ER sources ~~,~~ by estimating the $\delta^{13}C_{ER}$ ~~was estimated through Keeling plots using the same samples~~. We collected air samples in vertical profiles in October 2019 and December 2021 at the Amazon Tall Tower Observatory (ATTO) in the central Amazon. Air samples were collected in a diel cycle from two heights below ~~and one above~~ the canopy (4 ~~,~~ and 24 ~~, and~~ m agl). Afternoon above-canopy samples (79 ~~m agl, respectively)~~ and 321 m agl) were collected as background. For the campaign of October 2019, the mean $\Delta^{14}C_{ER}$ ~~was 33.9 ± 7.7~~ ranged from 24 ‰ ~~using the Keeling plot method, and 31.6 ± 7.5~~ to 41 ‰ with ~~the~~ both Keeling and Miller-Tans ~~method~~methods. In December 2021, mean $\Delta^{14}C_{ER}$ ~~was 77.0 ± 28.3~~ ranged from 53 ‰ ~~using the Keeling plot method, and 77.9 ± 24.0~~ to 102 ‰ ~~with the Miller-Tans method~~. The $\delta^{13}C_{ER}$ showed a smaller variation, being -27.8 ± 0.3 ‰ in October 2019 and -29.0 ± 0.5 ‰ in December 2021. ~~Combining the~~ The $\Delta^{14}C_{ER}$ estimates were compared with the record of atmospheric radiocarbon from the bomb period, ~~we obtained estimates of the~~ providing estimates of mean transit time of 6 ± 2 years for 2019 and 18 ± ~~5~~ 4 years for 2021. In contrast to steady-state carbon balance models that predict constant mean transit times, these results suggest an

important level of variation in mean transit times. ~~Nevertheless, new carbon fixed in this~~ We discuss these results in the context of previous model-based estimates of mean transit time for tropical forests and the Amazon region. In addition, we discuss previous studies that indicate that approximately 70% of assimilated carbon is respired as autotrophic respiration in the central Amazon. Our results suggest that newly fixed carbon in this terra-firme tropical forest is respired ~~, on average, in one or~~ within one to two decades, ~~which means~~ implying that only a fraction of ~~the~~ assimilated C can act as a sink for decades or longer.

1 Introduction

Tropical forests play a relevant role in the global carbon (C) cycle for two main reasons: (i) due to their high assimilation rate of carbon dioxide (CO_2) through photosynthesis (gross primary production, GPP, at ecosystem level; Beer et al. (2010); Jung et al. (2020)); and (ii) their high storage of C in vegetation and soils, representing up to a quarter of total C mass in terrestrial ecosystems (Carvalhais et al., 2014; Malhi et al., 2011).

In particular, the Amazon rainforest, as the largest continuous rainforest in the world, plays an important role in the global C cycle, taking up significant amounts of CO_2 from the atmosphere (Stephens et al., 2007; Malhi et al., 2015; Phillips and Brienen, 2017; Baker and Spracklen, 2019; Botía et al., 2022), and storing this carbon in terrestrial ecosystems for times that can range from hours to centuries (Sedjo and Sohngen, 2012; Sierra et al., 2021a).

Although the rates of C uptake in Amazon forests are among the largest in ~~land photosynthesis~~ terrestrial ecosystems (Malhi et al., 1999), C losses through respiration are also very high ~~(Chambers et al., 2004; Malhi et al., 2011) and might compensate~~ and autotrophic respiration is estimated in around two-thirds of assimilated C in the central Amazon, compensating most of the C uptake ~~(Sierra et al., 2007; Chambers et al., 2013)~~(Chambers et al., 2004; Sierra et al., 2007; Malhi et al., 2011; Chambers et al., 2013) . Additionally, several studies have found high variability in the magnitude and direction of C fluxes in the Amazon region because of anthropogenic disturbances (e.g. fires and deforestation) and extreme drought events (e.g. associated with El Niño) (Brienen et al., 2015; Phillips and Brienen, 2017; Hubau et al., 2020; Gatti et al., 2021). Therefore, to better understand the overall carbon balance of the Amazon forests, it is not only important to know the amount of carbon uptake, but also for *how long* C is retained within these ecosystems (Muñoz et al., 2023). ~~There is a need for an integrating quantity that gives information on how long the C stays in the system under both equilibrium and disturbance conditions.~~

A key diagnostic metric for characterizing timescales of C cycling in ecosystems is the transit time of C, which can be defined as the age of C in ecosystem respiration (Rasmussen et al., 2016; Sierra et al., 2017; Lu et al., 2018). The total respiration flux of an ecosystem is composed of C that spends different amounts of time stored in different ecosystem compartments (Trumbore, 2006), and it captures the metabolic activity of both autotrophic and heterotrophic organisms. Therefore, the age of C in ecosystem respiration, i.e. the transit time of C through the ecosystem, serves as a key diagnostic metric to characterize how long on average C atom is stored in ecosystems before it is respired back to the atmosphere as CO_2.

Radiocarbon (^{14}C) can be used as a tracer of C dynamics in ecosystems and to track how C moves across different ecosystem C pools. Measurements of radiocarbon in respiration can also be used to quantify the transit time of C through ecosystems (Trumbore and De Camargo, 2009). ~~Nuclear~~ Radiocarbon is produced naturally in the upper atmosphere by the interaction of

thermal neutrons from cosmic rays with ^{14}N in the atmosphere. Additionally, nuclear weapon tests in the atmosphere during the late 1950s and early 1960s produced a large number of thermal neutrons that led to the production of excess ^{14}C. After the natural and anthropogenic production, ^{14}C is oxidized to CO_2 and is incorporated into the global carbon cycle. After the Limited Test Ban Treaty in 1963, the concentration of radiocarbon $^{14}CO_2$ in the atmosphere started to decline due to its incorporation in the biosphere and surface ocean (Levin et al., 2022). Atmospheric CO_2 containing amounts of ^{14}C that change changes over time since the 1960s is assimilated by terrestrial ecosystems in the same manner as natural isotopes of C. For instance, CO_2 C in freshly fixed plant metabolites (e.g. leaf sugars) will have the same ratio of ^{14}C to total C ($^{14}C/C$, total C = $^{12}C + ^{13}C + ^{14}C$) content as the atmosphere at the time they were assimilated; similarly, CO_2 respired by fast-cycling pools (e.g. leaves) should have $^{14}C/C$ close to the contemporaneous atmospheric $^{14}C/C$ signal. Yet ^{14}C respired from organic matter decomposition would reflect the age of C used to grow plant tissue plus the time it takes for decomposition - leading to organic matter C ages , leading to C ages of respiration from organic matter generally higher than one year. CO_2 respired by fast-cycling pools (e.g. canopy leaves) should have ^{14}C isotopic signature close to the contemporaneous atmospheric ^{14}C signal. Thus, the age of C in ecosystem respiration is a mix of ages of C respired from different compartments with distinct isotopic signatures and reflects integrates the timescales of different processes such as production, allocation, and decomposition (Trumbore and De Camargo, 2009; Chanca et al., 2022).

An estimate of the whole ecosystem respiration ^{14}C /C isotopic ratio can be obtained from the covariation of ^{14}C with CO_2 concentration in the air using end-member mixing analysis methods such as the Keeling plot (Keeling, 1958, 1961) or the Miller-Tans plot (Miller and Tans, 2003) methods. Traditionally, Keeling plots have been applied to terrestrial ecosystems to characterize the stable C isotopic signatures of the main sources of ecosystem respiration that have different $\delta^{13}C$, i.e. the deviation in parts per thousand of sample $^{13}C/^{12}C$ in comparison to a standard material (Pataki et al., 2003), but the method can also be used to obtain the radiocarbon signature of ecosystem respiration (Phillips et al., 2015). Comparison between the mean ^{14}C /C value isotopic signature of the whole ecosystem respiration and the time history of the ^{14}C /C isotopic signature in atmospheric CO_2 provides an estimate of the mean transit time for C, i.e. the time C takes to move through the whole ecosystem from photosynthesis to respiration.

Based on two end-member isotope We used isotopic mixing models of radiocarbon in atmospheric CO_2 below and above the canopy level , we address here the to address two questions:

(i) What is the mean transit time of C for an Amazon terra-firme forest estimated with Keeling /and Miller-Tans methods using $^{14}CO_2$?

(ii) How does this empirical estimate compare with other model-based estimates of mean transit time for tropical forests?

To address these questions, we provide first a brief introduction to end-member mixing analysis as applied for radiocarbon measurements in CO_2, describing the sampling sites and statistical methods. We then report our estimates of mean transit times and discuss the results in the context of previous model-based estimates of mean transit time for tropical forests and the Amazon region.

2 Materials and Methods

2.1 End-member mixing analysis

The Keeling plot and Miller-Tans plot methods are based on two conservation equations. First, it is assumed that the concentration of CO_2 below a forest canopy ($[CO_2]_{can}$) is the mix of CO_2 from a tropospheric background ($[CO_2]_{trop}$) and the CO_2 released from ecosystem respiration ($[CO_2]_{ER}$) (Equation 3). Second, isotopic mixing in CO_2 below the canopy is proportional to the concentration of CO_2 in the tropospheric background and in ecosystem respiration (Equation 4) (Tans, 1980). These assumptions lead to the following equations

$$[CO_2]_{can} = [CO_2]_{trop} + [CO_2]_{ER},$$

$$R_{can} \times [CO_2]_{can} = R_{trop} \times [CO_2]_{trop} + R_{ER} \times [CO_2]_{ER},$$

where R is the isotopic ratio of C in CO_2, expressed as δ^{13}C for the stable C isotopes, and as Δ^{14}C or F^{14}C for the ^{14}C isotope over total C. The δ^{13}C corresponds to:

$$\delta^{13}\mathrm{C} = \left(\frac{\left(\frac{^{13}\mathrm{C}}{^{12}\mathrm{C}}\right)_{sample}}{\left(\frac{^{13}\mathrm{C}}{^{12}\mathrm{C}}\right)_{standard}} - 1 \right) \times 1000\,[‰]$$

The Δ^{14}C notation is used to express the isotopic ratio ^{14}C/C with a correction for mass-dependent fractionation and radioactive decay. Specifically,

$$\Delta^{14}\mathrm{C} = \left(\mathrm{F}^{14}\mathrm{C}\; e^{\lambda(1950 - y_{meas})} - 1 \right) \times 1000\,[‰]$$

where $F^{14}C$ ($=\frac{A_{SN}}{A_{ON}}$) is the Fraction Modern – A_{SN} is the specific activity of the sample and A_{ON} is the specific activity of oxalic acid standard material (OxII), both normalized to $\delta^{13}C = -25‰$ with respect to the V-PDB standard; λ is the updated ^{14}C decay constant ($\frac{1}{8{,}267}\ yr^{-1}$), and y_{meas} is the year of measurement. Δ^{14}C is corrected for mass-dependent fractionation through AMS online δ^{13}C, assuming ^{14}C fractionates ca. twice as much as ^{13}C (Stuiver and Polach, 1977; Reimer et al., 2004) .

Using the mass conservation of equation (3), equation (4) can be reduced to

$$R_{can} = \frac{[CO_2]_{trop}}{[CO_2]_{can}} \times (R_{trop} - R_{ER}) + R_{ER}.$$

Equation (5) is in essence a linear equation of the form $y = ax + b$, where the independent variable x is $\frac{1}{[CO_2]_{can}}$; y is the isotopic signature observed in the canopy, R_{can}; $a = (R_{trop} - R_{ER})[CO_2]_{trop}$; and b, or hereafter the y-intercept, is R_{ER}, i.e.

the isotopic signature of CO_2 respired by the whole ecosystem. Using linear regression, the values of a and b can be obtained if the values of x and y are known. This approach for obtaining the isotopic signature of a source in a two end-member mixing model is commonly known as the Keeling plot method (Keeling, 1958). In this study, we are interested in particular in the radiocarbon signature of ecosystem respiration, which we express as $\Delta^{14}C_{ER}$ or $F^{14}C_{ER}$.

Notice that equation 4 leads to the requirement that the background signal does not change over time (Equation 5) (Keeling, 1958, 1961) . Miller and Tans (2003) rearranged equation (4) obtaining the following equation:

$$R_{can} \times [CO_2]_{can} - R_{trop} \times [CO_2]_{trop} = R_{ER}([CO_2]_{can} - [CO_2]_{trop}),$$

which can also be expressed as a linear function where the intercept b equals zero; x is $([CO_2]_{can} - [CO_2]_{trop})$, i.e. the difference between CO_2 concentrations below and above canopy; y is $R_{can} \times [CO_2]_{can} - R_{trop} \times [CO_2]_{trop}$; and the slope a is R_{ER}, i.e. the isotopic signature of ecosystem respiration.

Such rearrangement removes the requirement of a constant background over time in the Keeling-plot approach. However, it requires the variation over time of background concentrations and C isotope ratio to be known.

Because of the correction for mass-dependent fractionation, both $\Delta^{14}C$ and $F^{14}C$ do not reflect effects of isotope fractionation. The variations in the radiocarbon signature will be related to the age of the carbon. To estimate the time between C assimilation and release from the ecosystem (mean transit time), one can compare the obtained value of $\Delta^{14}C_{ER}$ with records of atmospheric $\Delta^{14}C$-CO_2 for the study region. The difference between the year of collection of the subcanopy $^{14}CO_2$ and the equivalent calendar years where $\Delta^{14}C_{ER}$ = atmospheric $\Delta^{14}C$-CO_2, translates into an estimate of mean transit time in units of years.

2.1 Study site

Atmospheric air samples below and above the canopy level were collected at an 80 m tall walk-up tower (coordinates (WGS 84): 02°08.6470′S, 58°59.9920′W) located at the Amazon Tall Tower Observatory (ATTO) site, in the Uatumã Sustainable Development Reserve, in the central Amazon. The ATTO site is located ca. 150 km NE of the city of Manaus, and also counts with two more . In addition, the site includes two other towers: the ATTO tall tower (02°08.7520′S, 59°00.3350′W; 325 m tall) and a triangular mast (02°08.6020′S, 59°00.0330′W; 81 m tall) (Andreae et al., 2015). Meteorological conditions are measured continuously at the 80 m walk-up tower.

The three towers are located on a plateau area, with vegetation characterized as old-growth closed-canopy *terra-firme* (non-flooded) forest. Around the towers, the canopy rises to approximately 35 m with emergent trees achieving 45 m aglabove ground level (agl). Areas surrounding the tower include a network of plateaus and valleys connected by relatively steep slopes with a maximum relief height of ca. 100 m, with the base of the tall tower being located at an elevation of 120 m above sea level (asl) (Andreae et al., 2015).

The mean annual precipitation measured locally between the years 2012 and 2019 was 1934.1 mm yr^{-1}(Botía et al., 2022). Mean air temperatures do not vary strongly in the central Amazon, including the ATTO site. However, temperature maxima at the canopy level may vary between seasons. During the dry season (August – November), the daytime temperature maxima at

the canopy top are slightly above 30 °C. During the wet season (February – May) the daytime temperature maxima are around 28 °C. In both seasons, the temperature minima are around 22 °C (Andreae et al., 2015).

2.2 Sampling

Forest air samples were collected from two heights within the canopy at 4 and 24 m agl, in two campaigns during the dry and transition of dry-to-wet seasons. The first campaign took place in October 2019, and the second campaign in December 2021. ~~In both campaigns, a~~ A few samples were collected from the top level of the 80 m walk-up tower (79 m agl) to be used as a reference ~~for above canopy air , when flasks from the top level of~~ of the above-canopy air for the Miller-Tans plots, which consists of an approach where the values (Δ^{14}C-CO_2, CO_2 concentrations) observed within the canopy are plotted after subtraction of the ~~tall tower (321 m agl) were not available. In 2019 samples of air below the canopy were collected following a 24 hour cycle with sampling times roughly every two hours between 05 October and 06 October, totaling 20 sub-canopy samples. Including the samples collected at~~ values observed in the tropospheric background (Miller and Tans, 2003). The canopy level at the study plot is around 35 m high, making the 79 m ~~, a total of 24 samples were collected in October 2019. On 19 December and 20 December~~ level reasonably appropriate as a background (Pataki et al., 2003). At the ATTO tall tower, since September 2021, ~~samples were collected in intervals of three to four hours during the day and intervals of up to eight hours during the night, adding up to 12 samples. Flasks sampled between local sunrise (≈ 5:45) and local sunset (≈ 18:00) are considered daytime; otherwise, they are considered nighttime. During laboratory analyses, some samples failed quality control standards or flasks got broken, so the final data comprises 19 samples for October 2019 and 10 samples for December 2021. For samples collected in 2019, the year of measurement (y_{meas}, Equation 2)~~ air samples have been collected into flasks from 321 m agl. Additionally, since February 2019, one-month-integrated samples have been collected by absorption of CO_2 in NaOH solution for radiocarbon analysis ~~was 2020, and for samples collected in 2021, y_{meas} was 2023.~~ at 321 m through the method detailed by Levin et al. (1980).

Air from the different heights was collected through Synflex® metal/plastic composite tubings of 1/4" O.D. connected to the heights of 4, 24, and 79 m agl at the 80 m walk-up tower and 321 m agl at the ATTO tall tower. The air flowing from the tubing inlets was transferred to glass flasks of 3 L volume. The flasks contain valves of PCTFE seals and are the standard flasks of ICOS class-1 stations (Levin et al., 2020). Before shipment and sampling, flasks were conditioned (i.e. evacuated, baked, and filled with dry air) ~~. During collection, the 3 L flasks are pressurized with samples of local air at about 1.6 bar a (absolute)~~at the ICOS Central Analytical Laboratory.

At the 80 m walk-up tower, air samples were collected with a portable flask sampler, which is a compressor module that comprises a vacuum membrane pump/compressor and gauges for monitoring the flow of air and the pressure inside the flasks (Heimann et al., 2022). The aim is to pump air from the desired height into the flask, while simultaneously compressing the air to keep a final absolute pressure of about 1.6 bar inside the flask. Additionally, a drying agent can be attached to the system; the drying agent is particularly relevant when one is interested in the δ^{18}O-CO_2 (Steur et al., 2023), which was not our case. ~~However, when available, we used~~ Nevertheless, for the campaign of 2021, when the air relative humidity was high (dry-to-wet season), we decided to use anhydrous magnesium-perchlorate inside a cartridge before the flask to trap the water ~~vapor~~ vapour

from the air and avoid interferences on the airflow and eventual damage to the sampler due to water condensation on pieces of the equipment. Each sample was flushed for 15 minutes at a flow rate of ca. 2 L min^{-1}. Additional details on the standard flask sampling protocol at the Max Planck Institute for Biogeochemistry (MPI-BGC), as well as the flask sampling instructions for the portable sampler, can be found in Heimann et al. (2022).

At the ATTO tall tower, ~~flask samples are~~ air samples were collected with an ~~auto-sampler~~ automated sampler from the ICOS network (Levin et al., 2020) ~~. Additionally, one-month-integrated samples are collected by absorption of CO_2 in NaOH solution for radiocarbon analysis~~ from an inlet at 321 m ~~through the method detailed by Levin et al. (1980).~~

2.3 ~~Analytical methods and data analyses~~

~~The Miller-Tans model (Equation 6) consists of an approach where the values (Δ^{14}C-CO_2, CO_2 concentrations) observed within the canopy will be plotted after subtraction of the values observed in the tropospheric background. Thus, this method has been also called *canopy-minus-background* approach (Phillips et al., 2015). Defining and~~agl once per week between 13:00 and 14:00 local time (LT, UTC-0400) at a flow of 1~~/or measuring a representative background at the time of collectionfor the Miller-Tans plots is, therefore, crucial for obtaining accurate estimates of the $\Delta^{14}C_{ER}$~~t, which guarantees that the sample represents a real 1-hour mean air collection. During collection, the 3 L flasks are filled with samples of local air at about 1.6 bar absolute pressure.

Our reference background for CO_2 concentrations in 2019 consisted of flask samples taken at 79 m agl during the afternoon (13:29 and 17:09 LT). The ~~canopy level at the study plot is around 35 m height, making the 79 m level reasonably appropriate as a background (Pataki et al., 2003). Since September 2021, air samples have been collected into flasks from 321 m agl at the ATTO tall tower weekly between 13:00 and 14:00 LT at a flow of 1/t, which guarantees that the sample represents a real 1-hour mean ambient air collection. The~~ CO_2 concentration of a sample collected on 16 December 2021 was used as CO_2 background reference for the sub-canopy samples collected in December 2021. Background Δ^{14}C-CO_2 in October 2019 was based on a one-month integrated sample collected between 09 September 2019 and 15 October 2019. For the background Δ^{14}C-CO_2 in December 2021~~(Figure S1, supporting information)~~, two samples, collected during 24 November 2021 – 19 December 2021 and 19 December 2021 – 26 January 2022, were averaged.

~~The reference background for Δ^{14}C values (or equivalent F^{14}C) is based on radiometric analysis (low-level-counting) of radiocarbon from samples of CO_2 absorbed in a NaOH solution (Levin et al., 1980).~~ In 2019 samples of air below the canopy were collected following a 24 hour cycle with sampling times roughly every two hours between 05 October and 06 October, totaling 20 sub-canopy samples. Including the samples collected at 79 m, a total of 24 samples were collected in October 2019. On 19 December and 20 December 2021, samples were collected in intervals of three to four hours during the day and intervals of up to eight hours during the night, adding up to 12 samples. Flasks sampled between local sunrise (5:45) and local sunset (18:00) are considered daytime; otherwise, they are considered nighttime. During laboratory analyses, some samples were disregarded for being inconsistent with ambient air samples (e.g. SF_6 mole fraction equal to the one of the dry air used to fill the flasks for transport); additionally, some other flasks got broken, so the final data comprises 18 samples for October 2019 and 10 samples for December 2021.

2.3 Analytical methods and data analyses

CO_2 concentrations and C isotope ratios (δ^{13}C-CO_2 and Δ^{14}C-CO_2) from flask samples were measured in the laboratories (GasLab, IsoLab, and ^{14}C-Analytik) of MPI-BGC, in Jena, Germany, except for Δ^{14}C-CO_2 of samples collected in October 2019, whose values were determined by the Integrated Carbon Observation System – Central Radiocarbon Laboratory (ICOS-CRL) facility ~~at~~ in Heidelberg University, ~~in Heidelberg,~~ Germany, in collaboration with the Curt-Engelhorn-Zentrum Archäometrie (CEZA) AMS facility, in Mannheim, Germany.

The CO_2 concentrations inside the flasks were measured in the GasLab at MPI-BGC with an Agilent 6890 gas chromatograph equipped with an electron capture detector (ECD) and a flame ionization detector (Ni_{cat}-FID). Also in the MPI-BGC, δ^{13}C-CO_2 of air in the flasks was measured in the BGC IsoLab using a fully automated cryogenic extraction line ("BGC Airtrap"), coupled to the dual inlet system of a Finnigan MAT 252 stable isotope ratio mass spectrometer (IRMS, Thermo-Fisher Scientific, Bremen, Germany) (Heimann et al., 2022). Calibration was performed against the international "Jena Reference Air Set" (JRAS-06) scale (Wendeberg et al., 2013). The δ^{13}C (of CO_2) corresponds to

$$\delta^{13}\mathrm{C} = \left(\frac{\left(\frac{^{13}\mathrm{C}}{^{12}\mathrm{C}}\right)_{sample}}{\left(\frac{^{13}\mathrm{C}}{^{12}\mathrm{C}}\right)_{standard}} - 1 \right) \times 1000\,[‰] \quad (1)$$

The Δ^{14}C notation is used to express the isotopic ratio ^{14}C/C with a correction for mass-dependent fractionation and radioactive decay. Specifically,

$$\Delta^{14}\mathrm{C} = \left(\mathrm{F}^{14}\mathrm{C}\, e^{\lambda(1950 - y_{meas})} - 1 \right) \times 1000\,[‰] \quad (2)$$

where $F^{14}C$ ($=\frac{A_{SN}}{A_{ON}}$) is the Fraction Modern – A_{SN} is the specific activity of the sample and A_{ON} is the specific activity of oxalic acid standard material (OxII), both normalized to $\delta^{13}C = -25‰$ with respect to the V-PDB standard; λ is the updated ^{14}C decay constant ($\frac{1}{8{,}267}\ yr^{-1}$), and y_{meas} is the year of measurement. Δ^{14}C is corrected for mass-dependent fractionation through AMS online δ^{13}C, assuming ^{14}C fractionates ca. twice as much as ^{13}C (Stuiver and Polach, 1977; Reimer et al., 2004).

Δ^{14}C from CO_2 in air samples collected in flasks was determined after cryogenic extraction of CO_2 in a vacuum line and conversion to ~~$C_{graphite}$~~ graphite, which is the target of the Cs sputtering in the AMS both at CEZA and MPI-BGC. At the ICOS-CRL facility, ~~the~~ CO_2 extraction is performed using a dedicated automated Extraction and Graphitization Line (EGL) (Lux, 2018). At MPI-BGC the extraction of CO_2 for radiocarbon analysis follows the same principles of EGL. ^{14}C-to-C ratios at both CEZA and MPI-BGC are corrected for mass-dependent fractionation by δ^{13}C measurements in the AMS and calibrated against oxalic acid standard material (Ox-II).

The Δ^{14}C ~~from~~ values of the reference background (321 m agl) is based on radiometric analysis of radiocarbon from samples of CO_2 absorbed in a NaOH solution (Levin et al., 1980). Δ^{14}C from integrated air in NaOH samples were determined through low-level gas proportional counting at the Institute of Environmental Physics, in Heidelberg, Germany (Kromer and Münnich,

1992). For samples collected in 2019, the year of measurement (y_{meas}, Equation 2) for radiocarbon analysis was 2020, and for samples collected in 2021, y_{meas} was 2023.

2.4 ~~Reference atmospheric radiocarbon curve~~End-member mixing analysis

~~To obtain a mean transit time from the measured~~ The Keeling plot and Miller-Tans plot methods are based on two conservation equations. First, it is assumed that the concentration of CO_2 below a forest canopy ($[CO_2]_{can}$) is the mix of CO_2 from a tropospheric background ($[CO_2]_{trop}$) and the CO_2 released from ecosystem respiration ($[CO_2]_{ER}$) (Equation 3)(Keeling, 1958, 1961; Mill
. Second, isotopic mixing in CO_2 below the canopy is proportional to the concentration of CO_2 in the tropospheric background and ecosystem respiration (Equation 4) (Tans, 1980). These assumptions lead to the following equations

$$[CO_2]_{can} = [CO_2]_{trop} + [CO_2]_{ER}, \tag{3}$$

$$R_{can} \times [CO_2]_{can} = R_{trop} \times [CO_2]_{trop} + R_{ER} \times [CO_2]_{ER}, \tag{4}$$

where R is the isotopic ratio of C in CO_2, expressed as δ^{13}C for the stable C isotopes, and as Δ^{14}C or F^{14}~~C~~ ~~CO~~C for the ^{14}C isotope over total C.

Using the mass conservation of equation (3), equation (4) can be reduced to

$$R_{can} = \frac{[CO_2]_{trop}}{[CO_2]_{can}} \times (R_{trop} - R_{ER}) + R_{ER}. \tag{5}$$

Equation (5) is in essence a linear equation of the form $y = ax + b$, where the independent variable x is $\frac{1}{[CO_2]_{can}}$; y is the isotopic signature observed in the canopy, R_{can}; $a = (R_{trop} - R_{ER})[CO_2]_{trop}$; and b, or hereafter the y-intercept, is R_{ER}, i.e. the isotopic signature of CO_2 ~~signal ecosystemrespiration~~respired by the whole ecosystem. Using linear regression, the values of a and b can be obtained if the values of x and y are known. This approach for obtaining the isotopic signature of a source in a two end-member mixing model is commonly known as the Keeling plot method (Keeling, 1958). In this study, we are interested in particular in the radiocarbon signature of ecosystem respiration, which we express as $\Delta^{14}C_{ER}$ (and F^{14}C$_{ER}$ in the appendix).

Notice that equation 4 leads to the requirement that the background signal does not change over time (Equation 5) (Keeling, 1958, 1961) . Miller and Tans (2003) rearranged equation (4) obtaining the following equation:

$$R_{can} \times [CO_2]_{can} - R_{trop} \times [CO_2]_{trop} = R_{ER}([CO_2]_{can} - [CO_2]_{trop}), \tag{6}$$

which can also be expressed as a linear function where the intercept b equals zero; x is $([CO_2]_{can} - [CO_2]_{trop})$, i.e. the difference between CO_2 concentrations below and above canopy; y is $R_{can} \times [CO_2]_{can} - R_{trop} \times [CO_2]_{trop}$; and the slope a is R_{ER}, i.e. the isotopic signature of ecosystem respiration.

Such rearrangement removes the requirement of a constant background over time in the Keeling-plot approach. However, it requires the variation over time of background concentrations and C isotope ratio to be known.

Isotopic carbon signature of ecosystem respiration ($\delta^{13}C_{ER}$ and $\Delta^{14}C_{ER}$) were estimated with both Keeling and Miller-Tans approaches. Both end-member mixing models considered all the heights below and above the canopy, i.e. 4, ~~we need to use an atmospheric radiocarbon curve as a reference. However~~24, ~~the tropical region has not been continuously monitored for~~ 79 and 321 m and were not separated according to time of day. The results of the analyses were estimated by linear regressions fit with ordinary least squares (Model I regression) (Zobitz et al., 2006). We report the mean values with one standard error (σ) of the intercept obtained by the regressions in the Keeling approach and of the slope of the regression in the Miller-Tans approach. In both cases, we also report the 95% confidence interval (CI, ranging between percentiles 2.5 and 97.5).

Because of the correction for mass-dependent fractionation, both $\Delta^{14}C$ and F^{14}~~CO_2. Despite the lack of continuous data, here we use a~~ C do not reflect effects of isotope fractionation. The variations in the radiocarbon signature will be related to the age of the carbon.

2.5 Conversion to mean transit time and reference atmospheric radiocarbon

To obtain a mean transit time from the estimated ^{14}C signature of ecosystem respiration, it is necessary to use atmospheric radiocarbon data as a reference. We used a compilation of recently reported data by the CORSO project as a reference for the atmospheric radiocarbon data in our study region, which includes time series of atmospheric radiocarbon ~~data measured in~~ measured at research stations in the tropical region and surroundings. The data ~~included~~ used for the conversion of $\Delta^{14}C_{ER}$ into mean transit time ~~includes~~ included the stations BHD (Baring Head, New Zealand), CGO (Cape Grim, Australia), MER (Mérida Observatory, Venezuela) and SMO (Cape Matatula, Samoa) (Graven et al., 2012; Turnbull et al., 2017; Levin et al., 2010, 2022). The data was smoothed using curve fitting methods applied to time series in NOAA/ESRL/GMD (https://gml.noaa.gov/ccgg/mbl/crvfit/crvfit.html) (Thoning et al., 1989), accounting for interannual variability ~~. The~~ and it is reported in decimal years. The atmospheric $\Delta^{14}C$-CO_2 was averaged by year to have one value of $\Delta^{14}C$-CO_2 per year for the comparison with the year of collection of samples. The CORSO data is available in the Heidelberg University repository (https://heibox.uni-heidelberg.de/d/1f481155f63c46a8aaf0/) and the CORSO report with details of the collection and filtering of data is available on the ICOS Carbon Portal (https://meta.icos-cp.eu/objects/HnpnYFcQljQ-SJer66F-hr-b).

To estimate the time between C assimilation and release from the ecosystem (mean transit time), the $\Delta^{14}C_{ER}$ obtained from the intercept of the Keeling plot and slope of the Miller-Tans plot was compared to the subset of the CORSO data described above. The difference between the year of collection of the samples and the equivalent calendar years where $\Delta^{14}C_{ER}$ = atmospheric $\Delta^{14}C$-CO_2, translates into an estimate of mean transit time in units of years (yr). When $\Delta^{14}C_{ER}$ is not equal to atmospheric $\Delta^{14}C$-CO_2 of a given year, the calendar year with the closest atmospheric $\Delta^{14}C$-CO_2 to $\Delta^{14}C_{ER}$ is taken. Estimates of mean transit time are based on the variability of the mean $\Delta^{14}C_{ER} \pm \sigma$ (standard error of the linear regression), with the 95% confidence interval of the mean reported within parentheses.

2.6 Comparison with other approaches

The values of $\Delta^{14}C_{ER}$ obtained from end-member mixing analysis were converted to mean transit time and compared with predictions of two carbon balance models that can estimate the mean transit time of C in tropical ecosystems, and with an estimate of mean transit time produced from a synthesis of carbon and radiocarbon studies in the central Amazon region (Trumbore and De Camargo, 2009).

The first model is a simple one-pool model obtained as the total ecosystem C stock divided by the input GPP flux. This ratio provides an estimate of turnover time as reported by Carvalhais et al. (2014) for tropical forests at the global scale. The assumption of a one-pool model with this turnover time results in a probability distribution of turnover times that follows an exponential distribution with a mean equal to the turnover time (Metzler and Sierra, 2018). Because for a one-pool model, the age, turnover, and transit time of C are equal (Bolin and Rodhe, 1973; Sierra et al., 2017), we assume this distribution of turnover times is equivalent to the distribution of transit times.

The second model is a multi-compartmental model developed for the Porce region of Colombia (Sierra et al., 2021b). This model tracks the movement of C across seven ecosystem compartments, namely foliage, fine litter, wood, coarse woody debris, fine roots, coarse roots, and soil carbon (0 – 30 cm). It produces estimates of the transit time distribution of carbon assuming a constant GPP input flux of 24 ± 2 MgC ha^{-1} yr^{-1}.

A third estimate of a transit time distribution of C for tropical forests was obtained from the synthesis of carbon and radiocarbon studies of Trumbore and De Camargo (2009). These authors reported a mean age of ecosystem respired CO_2 of 3–7 yr. Their estimate was based on respiration fluxes, mean ages of C in CO_2 derived from decomposition of wood and roots, in addition to radiocarbon-based turnover times of soil carbon (Chambers et al., 2004; Vieira et al., 2005; Telles et al., 2003; Trumbore et al., 2006).

All computations were performed in the R environment (R v.4.2.2) using RStudio (version 2023.03.0+386).

3 Results

3.1 Keeling plots

We produced Keeling plots for both isotopes, δ^{13}C-CO_2 and Δ^{14}C-CO_2, and for the two separate sampling campaigns in 2019 and 2021. For δ^{13}C-CO_2, the intercept of the Keeling plot yielded a value of -27.8 $\pm$ 0.3 ‰ for October 2019, and a value of -29.0 $\pm$ 0.5 ‰ for December 2021 (Figure 1). The statistical fit of the data to the linear model was remarkably good, with the values of the R^2 coefficient ~~close~~ equal to 1.0.

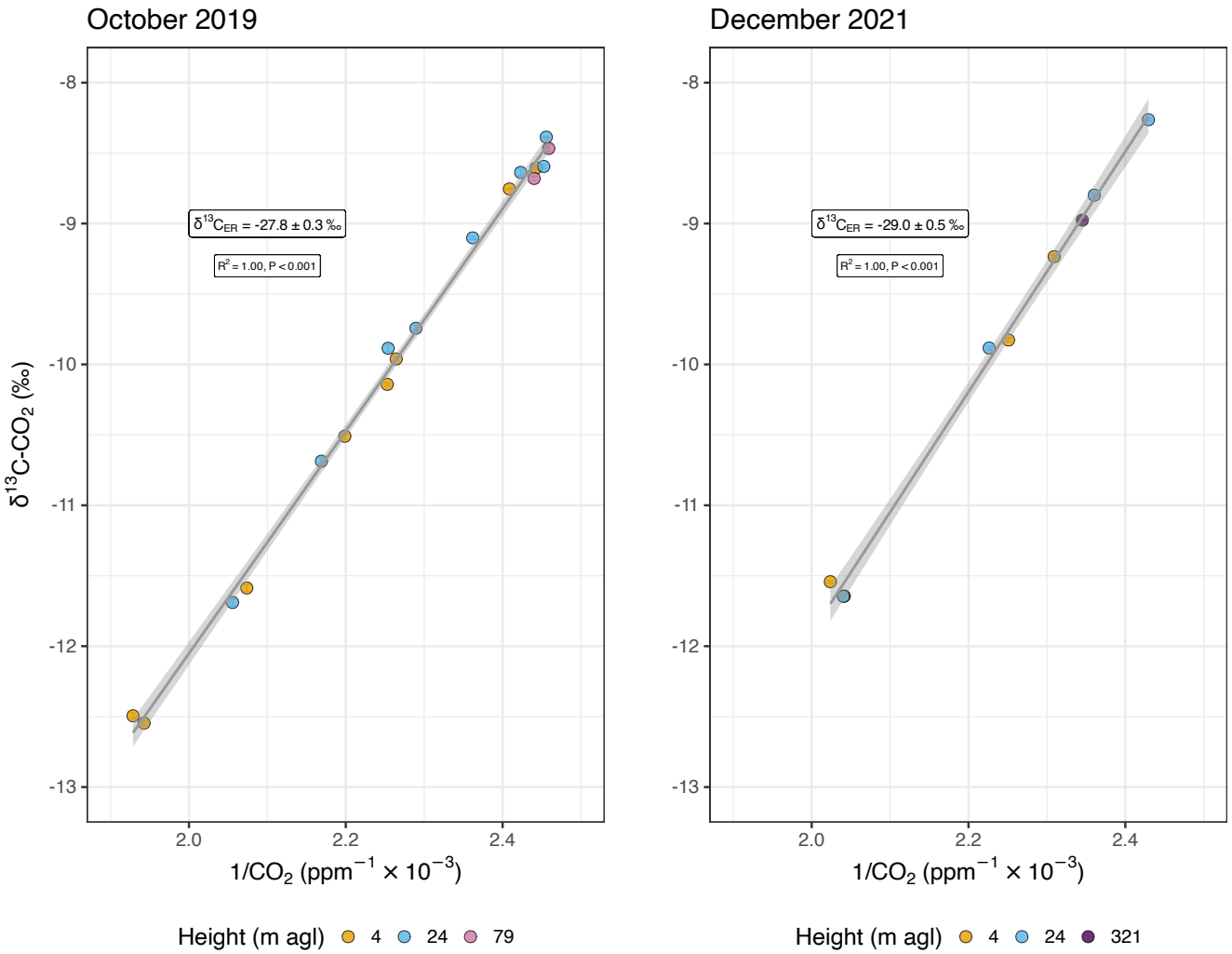

Figure 1. Keeling plot of δ^{13}C-CO_2 from below canopy (4 and 24 m agl) and above canopy (79 m agl) air for 5-6 October 2019 and 19-20 December 2021. Y-intercept ($\delta^{13}C_{ER}$) changes from -27.8 $\pm$ 0.3 ‰ to -29.0 $\pm$ 0.5 ‰. Analytical errors of δ^{13}C-CO_2 ranged from 0.005 to 0.04 ‰. Similarly, analytical errors of CO_2 vary between 0.01 and 0.3 ppm. Therefore, error bars are not easily visible in this scale.

The $\delta^{13}C_{ER}$ (i.e. y-intercept) obtained from the Keeling plots for October 2019 and December 2021 were significantly different (year predictor p-value < 0.001). ~~Despite the statistically significant difference, the $\delta^{13}C_{ER}$ did not change to values that could indicate a clear different respiration source altering the δ^{13}C signature of the whole ecosystem respiration.~~

The daytime CO_2-range (i.e. the difference between minimum and maximum concentrations over all heights) was ca. 111 ppm in October 2019, and in December 2021 it was slightly lower at 92 ppm. During nighttime, the CO_2-range was about 50 ppm in 2019 and 66 ppm in 2021 (Figure ~~S2~~S1, supporting information). The δ^{13}C-CO_2 mean value at nighttime was -10.5 ‰, which agrees well with the mean observed in 2019. ~~However, daytime~~ Daytime mean δ^{13}C-CO_2 was more enriched in

the heavier isotope (-9.3 ‰) ~~.~~, based on 13 daytime samples in 2019 and 4 daytime samples in 2021. Minimum values of δ^{13}C-CO_2 at daytime and nighttime are, nevertheless, very similar (-11.5 ‰ and -11.6 ‰, respectively).

Variability during day- and nighttime, and between sampling campaigns was much more pronounced for radiocarbon (Figure 2) than for δ^{13}C-CO_2. The statistical fit of the linear regression of the Keeling plot was relatively low for radiocarbon (R^2 = ~~0.40~~ 0.39 in 2019 and ~~0.48~~ 0.59 in 2021), although the obtained values of the intercepts were statistically significant ($p-$values = ~~0.003 and 0.018~~ 0.005 and 0.010 for 2019 and 2021, respectively).

~~Keeling-plot intercepts in $F^{14}C_{ER}$ were 1.0427 ± 0.0076 for October 2019 and 1.0811 ± 0.0258 for December 2021. In $\Delta^{14}C_{ER}$, the values were respectively 33.9 ± 7.7 ‰ and 71.6 ± 25.6 ‰ (Figure 3).~~ Δ^{14}C-CO_2 comprised a larger range of values in the second campaign, including more negative values at 24 m and higher maximum (18.4 ± 2.3 ‰) occurring at daytime (Figure 2). The minimum Δ^{14}C-CO_2 at daytime was -2.5 ± 2.2 ‰, while at nighttime it was -4.8 ± 2.2 ‰, both at 24 m. However, the ΔCO_2 was smaller in the second campaign, which implied a larger error in the Keeling plot, as a consequence of the extended extrapolation to obtain the y-intercept. $\Delta^{14}C_{ER}$ mean values and standard error were 33 ± 8 ‰ and 74 ± 21 ‰ in October 2019 and December 2021, respectively (Figure 3).

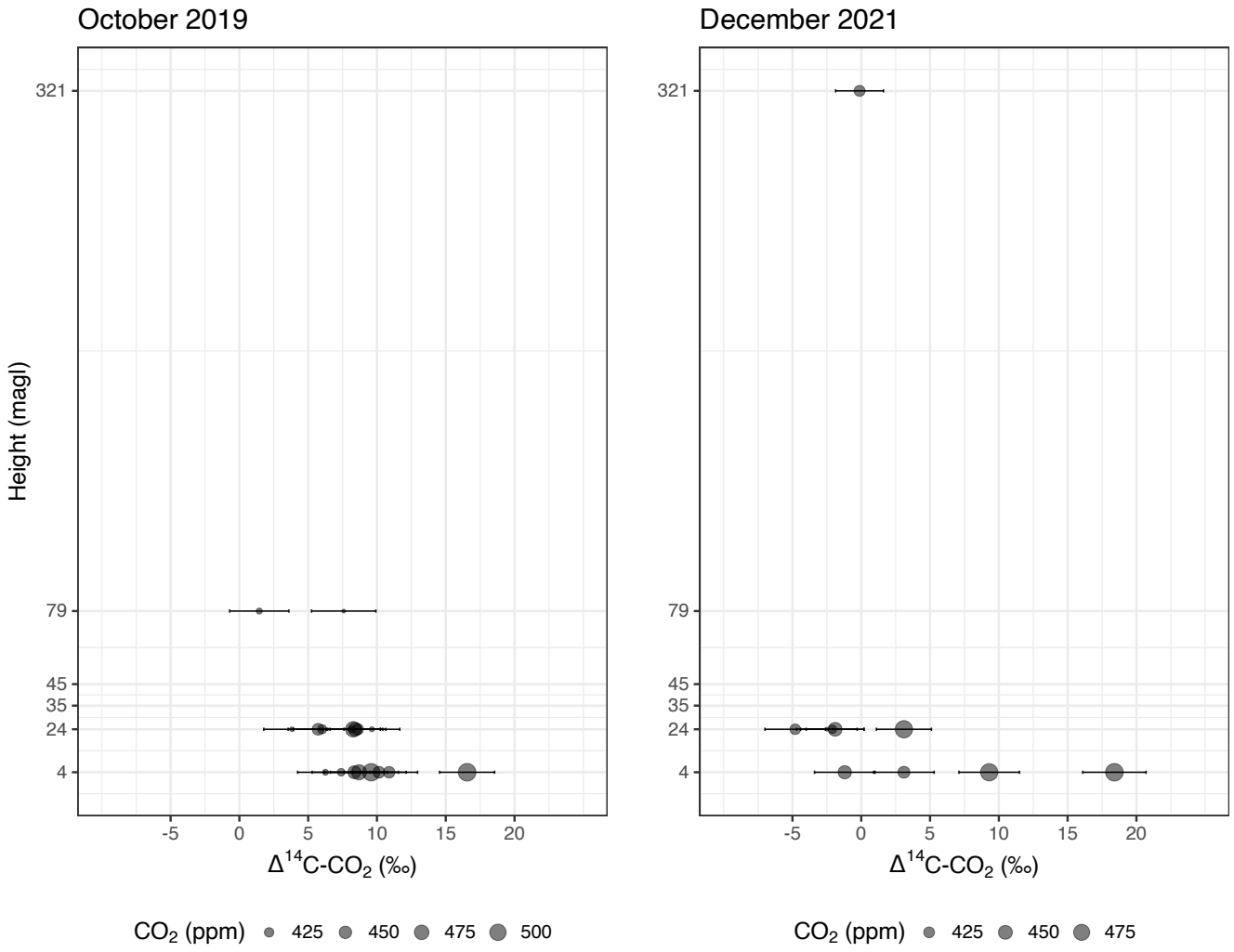

Figure 2. Distribution of values of Δ^{14}C-CO_2 and CO_2 concentrations according to the sampling heights below (4 and 24 m agl) and above (79 and 321 m agl) canopy. The canopy level in the study plot is around 35 m and some emergent trees occur at 45 m height. CO_2 concentration at 321 m is based on measurement from a flask and Δ^{14}C value is the average between two integrated samples (see main text). Analytical errors of Δ^{14}C-CO_2 measurements vary between 1.7 and 2.3 ‰.

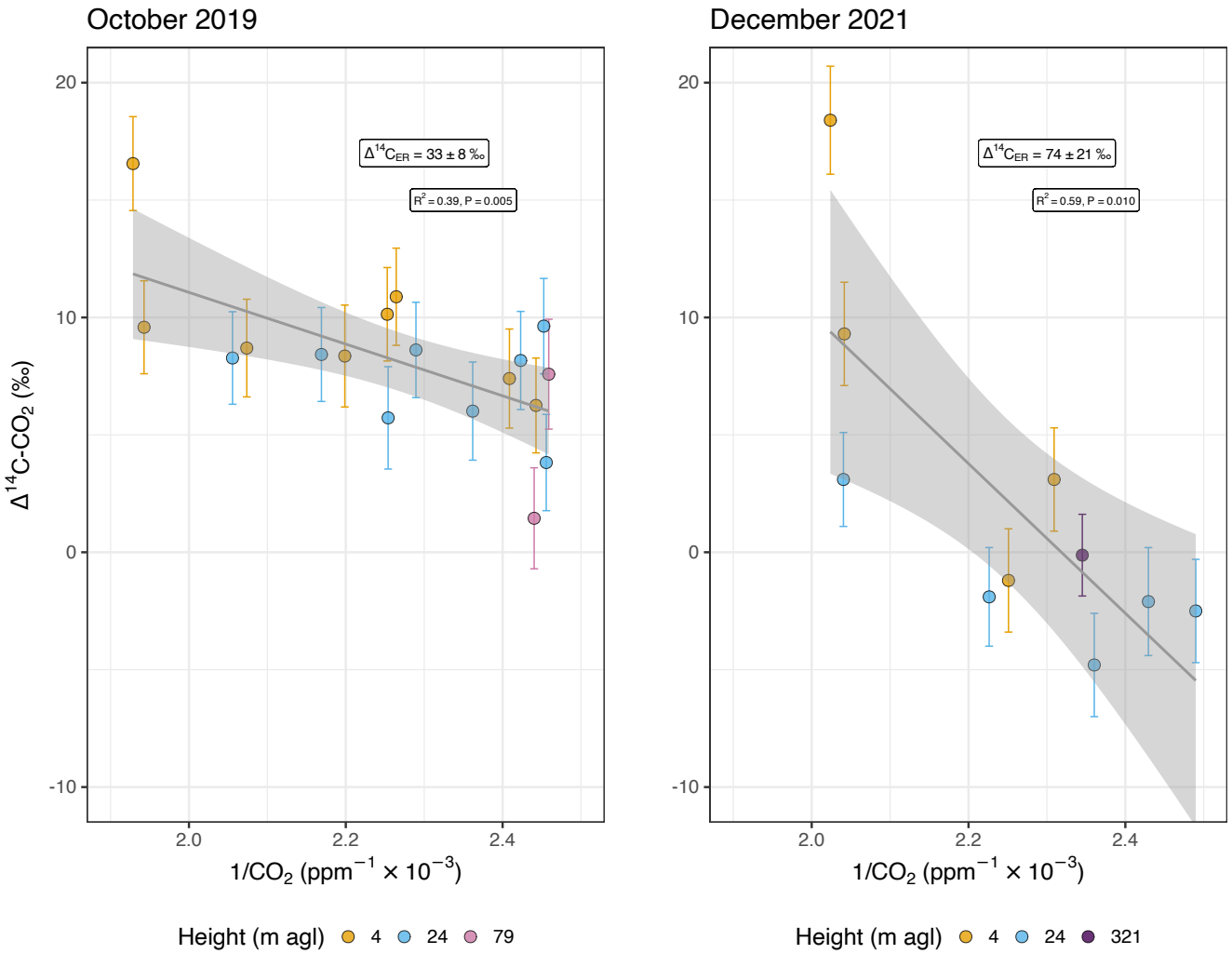

Figure 3. Keeling plot of Δ^{14}C-CO$_2$ for sampling campaigns in October 2019 and December 2021. ~~Y-intercept changes in $F^{14}C_{ER}$ from 1.0427 ± 0.0076 to 1.0813 ± 0.0240. In~~ $\Delta^{14}C_{ER}$ ~~, the~~ values change from ~~33.9~~ 33 ± ~~7.7~~ 8 ‰ to ~~77.0~~ 74 ± ~~28.3~~ 21 ‰. The light grey ribbon represents the ~~0.95~~ 95% confidence interval of the predictions.

3.2 Miller-Tans model

~~Even though there is a small variation in both CO_2 concentrations and δ^{13}C-CO_2 at 79 m, the estimates of $\delta^{13}C_{ER}$ are not significantly different between Keeling or Miller-Tans approaches (where background variation is explicitly incorporated), remaining at around -27.8 ± 0.3 ‰ for October 2019 and -29.0 ± 0.5 ‰ for December 2021. This is an indication that those variations did not qualify as a violation of the background stability for the Keeling plot method.~~

~~When available, our background reference consisted of samples collected at 321 m height. However, in 2019 we had no~~ The background CO_2 ~~concentrations at this height to be used as background in the Miller-Tans approach. Thus, an average of the CO_2 concentrations from two flasks collected on 05~~ concentration for October 2019 ~~at 13:29 and 17:09 (LT) at 79 m were assumed to represent the background for the diel samples of 05–06 October 2019. For the diel samples of 19–20 December 2021, the background is based on a flask sample collected on 16 December 2021 from 13:00 to 14:00 LT at 321 m. Therefore, the background CO_2 concentration for 05–06 October 2019~~ was 408.2 ppm (~~79 m height, n = 2,~~ σ = 2.2 ppm) ~~; and the~~ based on two flasks collected at 79 m in the afternoon because flask sampling at 321 m started only in 2021. The background CO_2 concentration for ~~19-20~~ December 2021 was 426.4 ppm (~~321 m height, n = 1,~~ σ = 0.002 ppm), based on one flask collected at 321 m. Based on continuous measurements in 2022, a daily variation of CO_2 is estimated ~~in~~ at ca. 34 ppm at 81 m and ca. 14 ppm at 321 m (Figure ~~S1~~S2, supporting information).

Alongside the small variation of the CO_2 concentrations at 79 m in 2019, δ^{13}C-CO_2 varied from -8.5 ‰ to -8.7 ‰. Nevertheless, the estimates of $\delta^{13}C_{ER}$ are not significantly different between Keeling or Miller-Tans approaches, despite the explicit incorporation of background variation in the latter method, remaining at around -27.8 $\pm$ 0.3 ‰ for October 2019 and -29.0 $\pm$ 0.5 ‰ for December 2021 (Miller-Tans plot not shown for δ^{13}C-CO_2).

Background Δ^{14}C-CO_2 is based on one-month integrated samples. For the campaign of October 2019, we ~~selected~~ used a sample collected between 09 September 2019 and 15 October 2019, with a Δ^{14}C-CO_2 of ~~7.9~~ 8 $\pm$ ~~1.6~~ 2 ‰. For the December 2021 campaign, two samples ~~, collected during~~ collected between 24 November 2021 ~~– 19 December 2021 and 19 December 2021 –~~ and 26 January 2022, were ~~used and their average~~ averaged providing a Δ^{14}C-CO_2 ~~is –0.1~~ equal to 0 $\pm$ ~~1.7~~2 ‰ (unpublished data). ~~Equation (2) was used to convert~~ The Miller-Tans-based mean Δ^{14}C~~into F^{14}C when needed, and the year of measurement for October 2019 is 2020, while for December 2021 it is 2023.~~

~~A linear model with the ordinary least squares method applied to both campaign's data separately provided an estimate of $F^{14}C_{ER}$ (slope of the linear regression) of 1.0403 $\pm$ 0.0076 for 05–06~~ 1σ was 32 $\pm$ 8 ‰ (15 – 48 ‰, 95% CI) in October 2019 and ~~1.0875~~ 78 $\pm$ ~~0.0242 for 19–20~~ 24 ‰ (21 – 135 ‰, 95% CI) in December 2021 (Figure 4). Estimates in F^{14}C are given in the appendix (Figure A1). ~~In Δ^{14}C, these values correspond to 31.6 $\pm$ 7.5 ‰ and 77.9 $\pm$ 24.0 ‰, respectively.~~

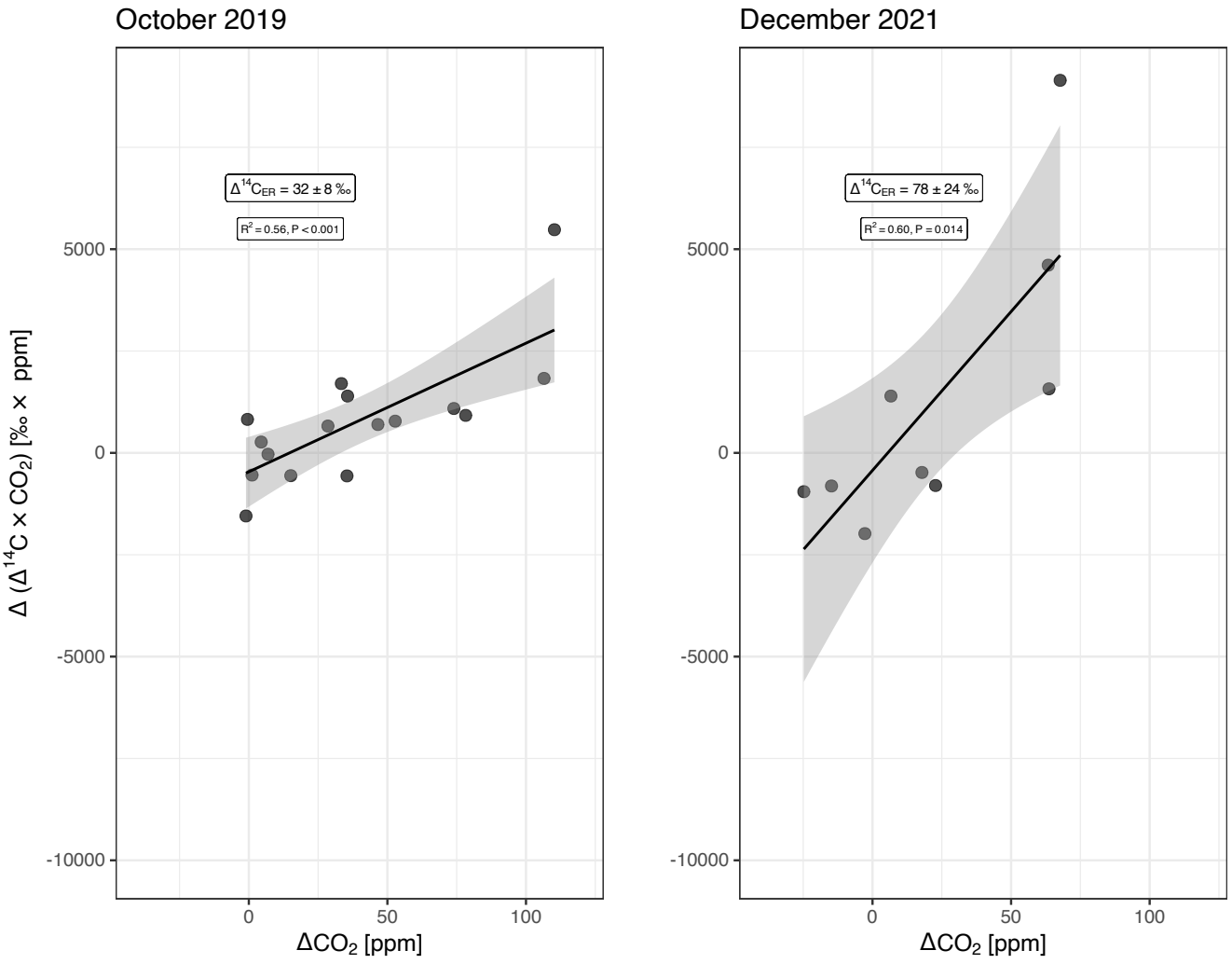

Figure 4. Miller-Tans model (with ordinary least squares regression) for October 2019 and December 2021. The light grey ribbon represents the ~~0.95~~ 95% confidence interval.

3.3 Estimates of ~~$\Delta^{14}C_{ER}$ and~~ mean transit time and comparison to other values from the literature

Our values of $\Delta^{14}C_{ER}$ obtained through end-member mixing analysis were ~~used in combination~~ compared with radiocarbon atmospheric records to estimate the mean age of the respired CO_2, in other words, the mean transit time of carbon.

The ~~Miller-Tans approach~~ Keeling plot for the campaign ~~on 05–06~~ in October 2019 results in a mean $\Delta^{14}C_{ER}$ ~~from 15.4~~ of 33 ‰ ~~to 47.7~~ with standard error of 8 ‰ (17 – 50 ‰, 95% CI) ~~. This interval in the bomb radiocarbon curve~~ that corresponds to the atmospheric $\Delta^{14}C$-CO_2 of the years 2015 to 2011 CE (common era) (2017 to 2008 CE, 95%CI) based on the CORSO data~~corresponds~~ . Thus, the corresponding mean age of respired CO_2 for the samples collected in October 2019, i.e. 2019

minus 2015 and 2019 minus 2011, is 4 – 8 yr (2 – 11 yr, 95% CI). The $\Delta^{14}C_{ER}$ based on the samples collected in December 2021 corresponds to the atmospheric $\Delta^{14}C$-CO_2 of years 2007 to 1999 CE (2015 to ~~2017 to 2008 CE (common era).~~ 1994 CE, 95% CI), which corresponds to a mean age of ecosystem respiration of 14 – 22 yr (6 – 27 yr, 95% CI).

The Miller-Tans approach for the campaign in October 2019 results in a $\Delta^{14}C_{ER}$ range that corresponds to the atmospheric $\Delta^{14}C$-CO_2 of the years 2015 to 2011 CE (2017 to 2009 CE, 95%CI) based on the CORSO data, i.e. a similar range as the Keeling plots. Thus, the corresponding mean age of respired CO_2 for the samples collected in October 2019 ~~is 2–11 years~~by Miller-Tans approach is 4 – 8 yr (2 – 10 yr, 95% CI). The $\Delta^{14}C_{ER}$ based on the samples collected ~~on 19-20~~ in December 2021 ~~ranges from 21.3 ‰ to 134.6 ‰ (~~corresponds to the atmospheric $\Delta^{14}C$-CO_2 of years 2007 to 1998 CE (2016 to 1993 CE, 95% CI), which corresponds to a mean age of ecosystem respiration of 14 – 23 yr (5 – 28 ~~years~~yr, 95% CI).

Estimates of the mean transit time of tropical ecosystems are available from three other approaches (Table 1). In the first approach (turnover time = stock-over-flux), Carvalhais et al. (2014) reported a mean turnover time of ~~11.6~~ 14 yr (12 – ~~18.2 yr (~~18 yr, 95% CI~~, mean = 14.2 yr~~) obtained as the ratio of the total C stock to GPP for tropical forests. It represents the mean of an exponentially distributed transit time distribution (Metzler and Sierra, 2018).

In a multi-compartmental approach, the transit time distribution reported from a 7-pool model for the Porce region of Colombia has a mean value of ~~11.2~~ 11 ± ~~1.2 years~~ 1 yr (Sierra et al., 2021b).

Based on a synthesis of carbon and radiocarbon data, Trumbore and De Camargo (2009) reported an average age of respired CO_2 weighted by the fluxes of different compartments (e.g. litter, wood) that ranged from 3 to 7 years for central Amazon forests near Manaus.

Table 1. Estimates of mean transit time of C for ATTO for the years 2019 and 2021 based on the conversion of $\Delta^{14}C_{ER}$ (mean values ± σ) into mean transit time of carbon. The mean transit time based on the 95% CI range is presented within parentheses. Comparison between different approaches, namely the end-member mixing ~~analysis~~ analyses of this study at the ATTO site (Keeling plot and Miller-Tans plot), and estimates for other sites and tropical regions. For steady-state systems, the estimate of the mean transit time of C does not change with the year. Turnover time as estimated by Carvalhais et al. (2014); 7-pool model computed by Sierra et al. (2021b); and data synthesis made by Trumbore and De Camargo (2009).

		Mean transit time (95% CI) [yr]	
Method	Study site	October 2019	December 2021
Keeling plot	ATTO site, Brazil	~~5~~ 4 – ~~9~~ 8 (2 – 11)	~~12~~ 14 – ~~24~~ 22 (6 – 27)
Miller-Tans plot	ATTO site, Brazil	4 – 8 (2 – 10)	~~13~~ 14 – 23 (5 – 28)
Turnover time	Tropical forests, worldwide	14 (12 – 18)	
7-pool model	Porce region, Colombia	10 – 12	
Data synthesis	Central Amazon, Brazil	3 – 7	

4 Discussion

4.1 What is the mean transit time of C for an Amazon terra-firme forest estimated with Keeling ~~/~~and Miller-Tans plots of $^{14}CO_2$?

We ~~were able to obtain estimates of~~ estimated the mean transit time of C for a tropical forest ecosystem using Keeling and Miller-Tans plots from field measurements of ^{14}~~CO~~C-CO_2. Although Keeling plots have been successfully used over decades to characterize the δ^{13}C signature of ecosystem respiration (e.g. Ehleringer and Cook, 1998; Knohl et al., 2005; de Araújo et al., 2008; Mauritz et al., 2019), the method has been rarely used with $^{14}CO_2$. The Miller-Tans approach with radiocarbon was used previously to understand biogenic and fossil sources contributing to the atmospheric air in urban environments (Miller et al., 2020). To our knowledge, the study of Phillips et al. (2015) was the first that combined isotope mixing analysis with $^{14}CO_2$ measurements to estimate the age of respired carbon in a temperate forest ecosystem.

Our approach provided estimates of mean transit time in a range from 2 to ~~30 years~~ 28 years (95% CI), differing depending on the sampling campaign. These estimates of mean transit time suggest that the carbon fixed during photosynthesis in these tropical forests is respired, on average, within one to three decades. The ~~results~~ $\delta^{13}C_{ER}$ estimated through the Keeling plot is equal to the estimate obtained through the Miller-Tans plot (where the background is explicitly incorporated). The similarity of $\delta^{13}C_{ER}$ estimates in both methods suggests that the small variations in CO_2 concentrations and δ^{13}C-CO_2 ~~Keeling plots~~ at 79 m were small enough not to violate the implicit assumption of a stable background in the Keeling plot method. The results of $\delta^{13}C_{ER}$ suggest that the source of ecosystem respiration ~~may have~~ has shifted between the two sampling campaigns from a value of -27.8 $\pm$ 0.3 ‰ in 2019 to a more depleted value of -29.0 $\pm$ 0.5 ‰ in 2021 ($p < 0.001$ with year as a predictor). These changes in δ^{13}C-CO_2 are known to occur in the Amazon region due to changes in precipitation (Ometto et al., 2002; Pataki et al., 2003)~~, which~~ . Assuming that the environmental factors altering δ^{13}C-CO_2 are also responsible for the changes in the Δ^{14}C-CO_2, the observed difference in $\delta^{13}C_{ER}$ may help to explain the differences in mean transit time we observed among the two field campaigns. Changes in other environmental factors such as ~~light availability and temperature~~ soil moisture may have also contributed to this ~~variability~~ difference in mean transit times~~(Lu et al., 2018).~~ . Chambers et al. (2004) have demonstrated that, for example, high soil respiration fluxes correlate with low soil moisture levels in the central Amazon. Furthermore, changes in the composition of pools contributing to respired C can alter its C transit time (Lu et al., 2018). Meteorological data from the 80-m walk-up tower shows that precipitation and soil water content were higher during the campaign of December 2021 than in the campaign of October 2019 (Figures S4, and S6, supporting information).

~~Moreover, in~~ Allowing the ~~method we used here, background concentrations of CO_2 and isotopes are particularly important for two reasons: (i)allowing the~~ background to vary (Miller-Tans approach) requires knowing well its values of Δ^{14}C-CO_2 and CO_2 concentration during the sampling period~~; (ii) the estimate of mean transit time is done by comparison with long-term records of Δ^{14}C-CO_2 in the background atmosphere (bomb curves). For (i)~~ . In this study we used a few afternoon samples from the height ~~of~~ at 79 m agl, which despite being reasonable, may still not be the best option for our fits, especially because it does not cover the whole sampling period. The measurements from 321 m agl are closer to an actual background, however, the resolution of one month in those samples could impair our ability to distinguish small variations that we may have captured in

our 2-day campaigns. ~~Nevertheless, by combining both types of samples we believe to have overcome the limitation of having only a few data points for an atmospheric background in this Amazon forest.~~

~~Point (ii) above implies~~ Moreover, the estimate of mean transit time is done by comparison with long-term records of Δ^{14}C-CO_2 in the background atmosphere. This implies the need for a time series of Δ^{14}C-CO_2 representative of the study region. Even though the division of regions in the bomb curve (Hua et al., 2022) is a useful guide, ~~again,~~ direct measurements of Δ^{14}C-CO_2 are still largely lacking in the Amazon region. Moreover, the atmospheric dynamics over the Amazon Basin are not trivial (Ancapichún et al., 2021), and the location of ATTO is influenced by mixed sources throughout the year (Botía et al., 2022).

Based on back-trajectory footprint analysis, the air circulation over ATTO between 80 m and 1000 m asl is highly influenced by the oscillation of the Intertropical Convergence Zone (ITCZ). During the wet season (February – May), the air masses predominantly follow a northeastern path, while during the dry season (August – November), the dominant wind directions come from the southeast, where the arc of deforestation is located in Brazil (Pöhlker et al., 2019; Saturno et al., 2018). The ITCZ influences the air movement over ATTO also during the dry to wet (December – January) and wet to dry (June – July) seasons, making the ATTO site meteorologically located in the Northern Hemisphere (NH) during the former and meteorologically in the Southern Hemisphere (SH) during the latter (Andreae et al., 2015). According to the division of zones proposed by Hua et al. (2022), which also takes into account the ITCZ patterns, the ATTO site would be located in SH Zone 3. However, the patterns of air movement above the central Amazon suggest that a mixed curve (Marsh et al., 2018) must be more appropriate when estimating mean transit times based on Δ^{14}C-CO_2 in the central Amazon.

Keeling plots of Δ^{14}C-CO_2 (where no background subtraction is applied) differ from the Miller-Tans approach by a few per mille, which corresponds to 1 to 2 years in mean transit time considering a steady annual decline of 3 to 5 ‰ in atmospheric Δ^{14}C-CO_2. ~~That means the end-member mixing analysis chosen~~ This indicates that choosing between Keeling or Miller-Tans approaches for estimating the $\Delta^{14}C_{ER}$ ~~might not have a large impact on the~~ is not the main factor impacting the precision and accuracy of the mean transit time estimate based on observations of ^{14}C-CO_2 in a vertical subcanopy profile. ~~After all, the~~ The sample size and uncertainty of C isotopic ratio measurements may have a larger influence on the standard errors of the y-intercept or slope of the regression ~~line~~lines in the Keeling plot and Miller-Tans plot, respectively. The method of employing end-member mixing analysis to $^{14}CO_2$ measurements seems, thus, promising ~~especially~~ also for the tropical regions, alongside the temperate regions as demonstrated before by Phillips et al. (2015). Nevertheless, more work is needed to repeat the measurements with seasonal frequency in the Amazonian region and to obtain similar estimates in other tropical regions worldwide. Additional estimates of empirical mean transit time would better quantify spatial and temporal variations of the C mean transit time. Furthermore, they would help to understand whether variations in the mean transit time are due to interannual variability or a trend in shifting mean transit times in tropical terrestrial ecosystems (Sierra et al., 2023).

4.2 How does this empirical mean transit time compare to model estimates of transit time in the Amazon region?

We compared our observation-based results with three previous estimates of mean transit time for tropical forests: the ~~transit time distribution computed with a 7-pool model for the Porce region of Colombia (Sierra et al., 2021b; Chanca et al., 2022),~~

the apparent turnover time estimated by Carvalhais et al. (2014) from GPP and total carbon stocks, and the estimate of age of respired carbon from a synthesis of observations reported by Trumbore and De Camargo (2009) for the central Amazon region, and the mean value of a transit time distribution computed with a 7-pool model for the Porce region of Colombia (Sierra et al., 2021b; Chanca et al., 2022).

In two short campaigns as ours, the observed increase in the radiocarbon signature may be related to a short-term increase in the flux of one of the older respiration sources. Potential sources of radiocarbon that could be relevant by being large enough and with high radiocarbon contents are dead wood (either as standing dead trees or as coarse woody debris) or old soil organic matter that gets destabilized with high water contents during the rainy season. For the ATTO site, there is good evidence that shows strong differences in temperature, precipitation, solar radiation, and soil water content between the two sampling campaigns (Figures S3, S4, S5, and S6, supporting information), which may help to explain differences in transit times.

To evaluate changes in the isotopic signature of the main ER sources, the $\delta^{13}C_{ER}$ was estimated through Keeling plots using the same samples. The $\delta^{13}C_{ER}$ showed a smaller variation than $\Delta^{14}C_{ER}$, being -27.8 $\pm$ 0.3 ‰ in October 2019 and -29.0 $\pm$ 0.5 ‰ in December 2021. A similar variability of $\delta^{13}C_{ER}$ has been observed in a topographical gradient at the Reserva Cueiras, a site in the central Amazon ca. 80 km away from ATTO (de Araújo et al., 2008). In that case, the valleys presented more negative $\delta^{13}C_{ER}$ values than the plateau areas during the dry season. The variability observed by de Araújo et al. (2008) indicated a correlation between $\delta^{13}C_{ER}$ and the water vapor saturation deficit in air (D), which was more evident on the plateaus than on the valleys. In their study, a $\delta^{13}C_{ER}$ about 1 – 1.5 ‰ lighter was linked to a high D with low soil water contents, which resembles our campaign of October 2019 in comparison to December 2021.

Our data is spatially and temporally limited. Although the observed difference in $\delta^{13}C_{ER}$ is statistically significant, it is not possible to set apart the effects of seasonal variability or changes on the fluxes of the respiration sources on the C isotopic signatures.

Hence the observed differences in $\Delta^{14}C_{ER}$ and, thus, mean transit time, might be related to seasonal variabilities that cannot be fully assessed with sporadic campaigns. To effectively elucidate the underlying drivers of the variability in the mean transit time, more ecosystem respiration sampling for radiocarbon measurements (and $\delta^{13}C$ as ancillary) is needed.

The mean transit time for the campaign in 2021 agrees with the turnover time estimated by Carvalhais et al. (2014), however, the same does not hold for the campaign in 2019, when the mean transit time based on end-member mixing analysis is shorter. The approach of Carvalhais et al. (2014) to obtain a turnover time integrates over large temporal and spatial scales by incorporating gross primary production values and C stocks over several years and with a resolution of 0.5°. However, it does not discern between pools of different ages that contribute in varied proportions to the total respiration flux. Therefore, it cannot account for pools that have with different $\Delta^{14}C$, but can only provide an approximation of approximate the radiocarbon signature within a well-mixed total ecosystem respiration. The mean transit time for the campaign in 2021 agrees with the turnover time estimated by Carvalhais et al. (2014), however, the same does not hold for the campaign Moreover, some of the potential reasons for the mismatch in 2019 , when the mean transit time based on end-member mixing analysis is shorter. Some of the potential reasons include a seasonal variability of $\Delta^{14}C\text{-}CO_2$ in the central Amazon, different contributions of respiration sources from year to year due to climate variations, or even a poor representation of local measurements in a short-

term campaign in comparison to the dynamics of the whole Amazon rainforest. ~~To overcome the different possibilities, more~~ More studies in different seasons, targeting individual respiration sources, and covering larger temporal and spatial scales are needed to overcome these different possibilities. The comparison with other estimates of mean transit time, however, suggests that this metric might not be constant over time, even for old-growth forests in the central Amazon.

~~Other studies~~ In contrast, in sites close to Manaus~~estimated respiration fluxes, mean ages of C of decomposing wood and roots, as well as turnover times of soils based on radiocarbon data (Chambers et al., 2004; Vieira et al., 2005; Telles et al., 2003; Trumbore e . Such information was summarised by Trumbore and De Camargo (2009) into an estimate of the mean time lag between photosynthetic assimilation and ecosystem C release through respiration. This time lag can be compared to our estimate of mean transit time based on $\Delta^{14}C_{ER}$, as both are defined similarly and either intrinsically or explicitly incorporate the path of C through interconnected multiple pools with different turnover times. Trumbore and De Camargo (2009)~~, Trumbore and De Camargo (2009 estimated a mean transit time of 3 to 7 years, which is similar to the value obtained by this study if we consider only the campaign of October 2019. The second campaign (December 2021) $\Delta^{14}C_{ER}$ generates a mean transit time of about ~~12 to 24~~ 14 to 23 years, which is about three times higher than the estimate by Trumbore and De Camargo (2009) for the central Amazon, however similar to the age estimate of 24 years by Fung et al. (1997) for heterotrophically respired C in broad-leaved evergreen tropical forests, also cited by Trumbore and De Camargo (2009). However, the model used by Fung et al. (1997) ~~presumed~~ assumed that 50% of C was respired autotrophically, with a third of the remaining 50% allocated to leaves, one-third to stems, and one-third to roots. In contrast, the study of respiration fluxes (Chambers et al., 2004) demonstrated that autotrophic respiration returned 70% of the C assimilated by a central Amazon rainforest to the atmosphere, so we expect the transit time estimate of Fung et al. (1997) to be systematically too long. Trumbore and De Camargo (2009) estimates were based on respiration fluxes, mean ages of C of decomposing wood and roots, as well as turnover times of soils based on radiocarbon data (Chambers et al., 2004; Vieira et al., 2005; Telles et al., 2003; Trumbore et al., 2006). Such information was summarised into an estimate of the mean time lag between photosynthetic assimilation and ecosystem C release through respiration. This time lag can be compared to our estimate of mean transit time based on $\Delta^{14}C_{ER}$, as both are defined similarly and either intrinsically or explicitly incorporate the path of C through interconnected multiple pools with different turnover times.

~~We argue that an empirical~~ A 7-pool model developed for a tropical forest in Colombia (Porce model) has a mean transit time of 10 to 12 years (Sierra et al., 2021b), which falls in between the mean transit time we estimated for October 2019 and December 2021. Therefore, it suggests that a multi-compartmental model estimates an average of the differences or trends of the ecosystem's mean transit time. The Porce model accounts for the C composition and C age structure of different compartments. A similar model for the central Amazon could be parameterised to account for the potential respiration sources that could drive the radiocarbon isotopic signature of ecosystem respiration by being large enough and with high radiocarbon contents such as dead wood (Chambers et al., 2004). This way, the empirical estimate of mean transit time can help to constrain a multi-compartmental model more representative of the central Amazon forest.

Our analysis shows that an empirical mean transit time based on forest air $\Delta^{14}C\text{-}CO_2$ coupled to isotope mixing analysis compares well with model estimates and other experimental approaches, at least for tropical forests. The ~~variability~~ differences from one year to the other or even between seasons ~~does not necessarily mean a limitation of the method, but a~~ imply a potential

natural variability of the weights of fluxes from different C pools with large differences in their turnover times. This variability could influence the C balance calculation in Amazon forests more than previously thought. In this sense, a practical method to calculate an ecosystem time metric such as transit time might improve our understanding of the C balance in Amazon forests and their role as C sources and sinks of atmospheric CO_2. This method also has the resolution to tackle temporal and spatial variabilities of the mean transit time of ecosystem respiration.

5 Conclusions

We obtained, for the first time in a tropical forest, an empirical estimate of a mean transit time of carbon of ecosystem respiration based on end-member mixing analysis of radiocarbon measurements of ambient and atmospheric CO_2. We estimate the mean transit time of carbon for a plateau area of a near-pristine central Amazon forest ranging from one to almost three decades. Our results suggest that a potentially large proportion of carbon assimilated through photosynthesis is released back ~~into~~ to the atmosphere relatively quickly. This could affect interpretations of the role of Amazon forests as a C sink or source.

Our results also showed that the age of respired carbon may be highly dynamic with important changes among seasons or years. This is in contrast to model-based estimates of transit time that often make the assumption of equilibrium and therefore cannot predict a time-dependent mean transit time. Potential reasons for the variability of transit times include (i) natural variation of ecosystem processes due to seasonality and inter-annual variability of environmental factors (e.g. changes in precipitation); (ii) human activities such as fire that release old carbon and affect atmospheric $\Delta^{14}C$-CO_2; (iii) high spatial and temporal heterogeneity in the sources of respired C at the ecosystem level. Hence it is essential to monitor the mean transit time of tropical ecosystems because it can change over time. Additionally, studies exploring the $^{14}CO_2$ respired by different components can help to define the underlying distribution of transit time of C that ~~, on one hand,~~ can have its mean value compared to the empirical estimate obtained through end-member mixing analysis. ~~On the other hand, the mean value of a non-normal distribution of the transit time of C alone cannot give accurate information on the short-term behavior of the ecosystem.~~

The method presented here was scarcely employed in the past and non-existent for an Amazon forest. However, this method has a large potential for understanding not only the source of respired carbon but also its age and the speed at which carbon is assimilated and respired by forest organisms. The method is particularly useful in tropical forests because of the large gradients and diurnal variations in the CO_2 concentration and its $\Delta^{14}C$ in the dense forest canopy. We showed that our sampling design was effective in obtaining a meaningful mean transit time of C with observations and isotope mixing analysis. Our mean transit time also compares well to other previous estimates based on models or data synthesis.

~~Our results also showed that the age of respired carbon may be highly dynamic with important changes among seasons or years. This is in contrast to model-based estimates of transit time that often make the assumption of equilibrium and therefore cannot predict a time-dependent mean transit time. Potential reasons for the variability of transit times include (i)natural variation of ecosystem processes due to seasonality and inter-annual variability of environmental factors (e.g. changes in~~

~~precipitation); (ii) human activities such as fire that release old carbon and affect atmospheric $\Delta^{14}C\text{-}CO_2$; (iii) high spatial and temporal heterogeneity in the sources of respired C at the ecosystem level.~~

Data availability. The CORSO data is available in the Heidelberg University repository (https://heibox.uni-heidelberg.de/d/1f481155f63c46a8aaf0/) and the CORSO report with details of the collection and filtering of data is available on the ICOS Carbon Portal (https://meta.icos-cp.eu/objects/HnpnYFcQljQ-SJer66F-hr-b). The analytical results of the flasks collected for this work are available on the ATTO data portal (https://www.attodata.org/) under the ID xxx (doi xxx) for the flasks collected in October 2019 and under the ID xxx (doi xxx) for the flasks collected in December 2021.

Appendix A: End-member mixing models with $F^{14}C$ notation

In other studies using Miller-Tans plots of $\Delta^{14}C\text{-}CO_2$, the context of interest has been to determine the fossil fraction in CO_2 emissions in urban areas (e.g. Miller et al. (2020)). In such contexts, $\Delta^{14}C\text{-}CO_2$ has values always below zero (down to -1000 ‰ if 100% fossil). On the other hand, ecosystem respiration can have a variety of $\Delta^{14}C\text{-}CO_2$ values, linked to the varied radiocarbon signatures of its sources. Therefore, in the context of this study, $\Delta^{14}C\text{-}CO_2$ can be positive (e.g. decomposition of old carbon with bomb signature), negative (pre-bomb or contemporaneous atmosphere), and zero (when the atmospheric value crosses from bomb ^{14}C signature to natural levels). In the Miller-Tans plots, the y-axis is the product of the C isotopic ratio by the CO_2 concentration (of the subcanopy values minus the background value) (Equation 6). Thus, in $\Delta^{14}C$ notation, a data point with a y-value equal to zero can be a consequence of (i) a subcanopy combination ($\Delta^{14}C \times CO_2$) equal to the current atmosphere or (ii) simply a $\Delta^{14}C$ equal to zero. Such ambiguity does not occur when $F^{14}C$ is instead used because $F^{14}C$ can only assume positive values. Calculating the Miller-Tans plot with $F^{14}C$ or $\Delta^{14}C$ does not change the value of the slope of the regression line, therefore it does not change the estimate of the mean transit time.

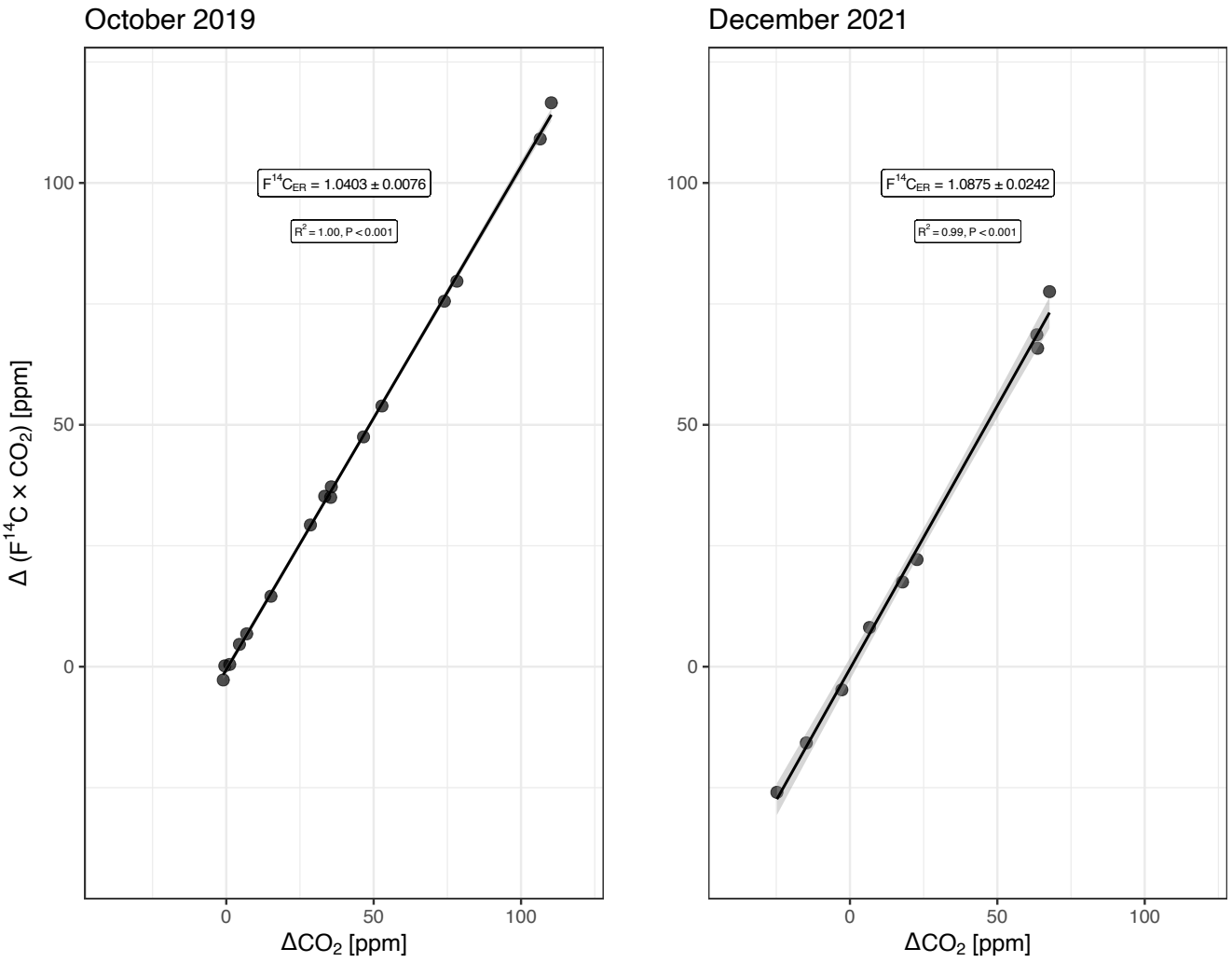

Figure A1. Miller-Tans model (with ordinary least squares regression) for October 2019 and December 2021. Slope of the regression line is the radiocarbon isotopic signature of the ecosystem respiration in $F^{14}C$ notation, i.e. $F^{14}C_{ER}$. $F^{14}C_{ER}$ = 1.0403 ± 0.0076 in October 2019 and $F^{14}C_{ER}$ = 1.0875 ± 0.0242 in Decembre 2021. The light grey ribbon represents the 95% confidence interval.

Author contributions. IC – Conceptualization, data curation, formal analysis, investigation, methodology, project administration, validation, visualization, writing - original draft preparation, writing - review and editing; IL – Conceptualization, data curation, formal analysis, funding acquisition, methodology, resources, supervision, validation, writing - review and editing; ST – funding acquisition, project administration, resources, supervision, writing - review and editing; KM – resources, supervision, writing - review and editing; JL – data curation, funding acquisition, methodology, resources, validation, writing - review and editing; CAQ – funding acquisition, project administration, resources, writing - review and editing; ACA – data curation, formal analysis, resources, validation, visualization, writing - review and editing; CQDJ

– data curation, formal analysis, resources, validation, visualization, writing - review and editing; HvA – data curation, formal analysis, resources, validation, visualization, writing - review and editing; SH – data curation, resources, validation, writing - review and editing; CS – Conceptualization, formal analysis, funding acquisition, methodology, project administration, resources, supervision, writing - review and editing.

Competing interests. The authors declare that they have no conflict of interest.

Acknowledgements. This work would not have been possible without the contribution and support of Prof. Dr. Ingeborg Levin (R.I.P.), who was working with us on finalizing the manuscript at the time of her death. All meetings and communications with her contributed to the definition of the experimental design, understanding of radiocarbon background data, interpretation of results, and several other aspects of this work. She is immortalized in the radiocarbon community for her wisdom, contributions, and endless support to the ones who had the honor of meeting her. Her support to the first author goes beyond the scientific realm and this acknowledgments section. The authors also would like to thank all the support provided by the ATTO team at the research site regarding the logistics of transport of material. Special thanks to Roberta Pereira de Souza, Yago Rodrigues Santos, Antônio Huxley Melo Nascimento, ~~Amauri~~ Amaury Rodrigues Pereira, and Nagib Alberto de Castro Souza. We also would like to thank personnel from ICOS-CRL and the central laboratories of the MPI-BGC, particularly Axel Steinhof, Heike Machts, Heiko ~~Moosen~~Moossen, Michael Rothe, Armin Jordan, and Steffen Knabe. This work and the Amazon Tall Tower Observatory (ATTO) project were funded by the German Federal Ministry of Education and Research (grant numbers 01 LK 1602 C and 01 LK 2101 A) and the Max Planck Society.

References

Ancapichún, S., De Pol-Holz, R., Christie, D. A., Santos, G. M., Collado-Fabbri, S., Garreaud, R., Lambert, F., Orfanoz-Cheuquelaf, A., Rojas, M., Southon, J., et al.: Radiocarbon bomb-peak signal in tree-rings from the tropical Andes register low latitude atmospheric dynamics in the Southern Hemisphere, Science of the Total Environment, 774, 145 126, https://doi.org/10.1016/j.scitotenv.2021.145126, 2021.

Andreae, M. O., Acevedo, O. C., Araùjo, A., Artaxo, P., Barbosa, C. G., Barbosa, H., Brito, J., Carbone, S., Chi, X., Cintra, B., et al.: The Amazon Tall Tower Observatory (ATTO): overview of pilot measurements on ecosystem ecology, meteorology, trace gases, and aerosols, Atmospheric Chemistry and Physics, 15, 10 723–10 776, 2015.

Baker, J. C. and Spracklen, D. V.: Climate benefits of intact Amazon forests and the biophysical consequences of disturbance, Frontiers in Forests and Global Change, 2, 47, 2019.

Beer, C., Reichstein, M., Tomelleri, E., Ciais, P., Jung, M., Carvalhais, N., Rödenbeck, C., Arain, M. A., Baldocchi, D., Bonan, G. B., et al.: Terrestrial gross carbon dioxide uptake: global distribution and covariation with climate, Science, 329, 834–838, 2010.

Bolin, B. and Rodhe, H.: A note on the concepts of age distribution and transit time in natural reservoirs, Tellus, 25, 58–62, 1973.

Botía, S., Komiya, S., Marshall, J., Koch, T., Gałkowski, M., Lavric, J., Gomes-Alves, E., Walter, D., Fisch, G., Pinho, D. M., et al.: The CO_2 record at the Amazon Tall Tower Observatory: A new opportunity to study processes on seasonal and inter-annual scales, Global Change Biology, 28, 588–611, 2022.

Brienen, R. J., Phillips, O. L., Feldpausch, T. R., Gloor, E., Baker, T. R., Lloyd, J., Lopez-Gonzalez, G., Monteagudo-Mendoza, A., Malhi, Y., Lewis, S. L., et al.: Long-term decline of the Amazon carbon sink, Nature, 519, 344–348, 2015.

Carvalhais, N., Forkel, M., Khomik, M., Bellarby, J., Jung, M., Migliavacca, M., Saatchi, S., Santoro, M., Thurner, M., Weber, U., et al.: Global covariation of carbon turnover times with climate in terrestrial ecosystems, Nature, 514, 213–217, https://doi.org/10.1038/nature13731, 2014.

Chambers, J. Q., Tribuzy, E. S., Toledo, L. C., Crispim, B. F., Higuchi, N., dos Santos, J., Araújo, A. C., Kruijt, B., Nobre, A. D., and Trumbore, S. E.: Respiration from a tropical forest ecosystem: partitioning of sources and low carbon use efficiency, Ecological Applications, 14, 72–88, https://doi.org/10.1890/01-6012, 2004.

Chambers, J. Q., Negron-Juarez, R. I., Marra, D. M., Di Vittorio, A., Tews, J., Roberts, D., Ribeiro, G. H. P. M., Trumbore, S. E., and Higuchi, N.: The steady-state mosaic of disturbance and succession across an old-growth Central Amazon forest landscape, Proceedings of the National Academy of Sciences, https://doi.org/10.1073/pnas.1202894110, 2013.

Chanca, I., Trumbore, S. E., Macario, K., and Sierra, C.: Probability distributions of radiocarbon in open linear compartmental systems at steady-state, Journal of Geophysical Research: Biogeosciences, 127, e2021JG006 673, https://doi.org/10.1029/2021JG006673, 2022.

de Araújo, A., Ometto, J., Dolman, A., Kruijt, B., and Ehleringer, J.: Implications of CO_2 pooling on $\delta^{13}C$ of ecosystem respiration and leaves in Amazonian forest, Biogeosciences, 5, 779–795, https://doi.org/10.5194/bg-5-779-2008, 2008.

Ehleringer, J. and Cook, C.: Carbon and oxygen isotope ratios of ecosystem respiration along an Oregon conifer transect: preliminary observations based on small-flask sampling, Tree Physiology, 18, 513–519, 1998.

Fung, I., Field, C., Berry, J., Thompson, M., Randerson, J., Malmström, C., Vitousek, P., Collatz, G. J., Sellers, P., Randall, D., et al.: Carbon 13 exchanges between the atmosphere and biosphere, Global Biogeochemical Cycles, 11, 507–533, 1997.

Gatti, L. V., Basso, L. S., Miller, J. B., Gloor, M., Gatti Domingues, L., Cassol, H. L., Tejada, G., Aragão, L. E., Nobre, C., Peters, W., et al.: Amazonia as a carbon source linked to deforestation and climate change, Nature, 595, 388–393, 2021.

Graven, H. D., Guilderson, T. P., and Keeling, R. F.: Observations of radiocarbon in CO2 at seven global sampling sites in the Scripps flask network: Analysis of spatial gradients and seasonal cycles, Journal of Geophysical Research: Atmospheres, 117, 2012.

Heimann, M., Jordan, A., Brand, W. A., Lavrič, J. V., Moossen, H., and Rothe, M.: The atmospheric flask sampling program of MPI-BGC, Version 13, 2022, Edmond – Open Research Data Repository of the Max Planck Society, https://doi.org/10.17617/3.8r, 2022.

Hua, Q., Turnbull, J. C., Santos, G. M., Rakowski, A. Z., Ancapichún, S., De Pol-Holz, R., Hammer, S., Lehman, S. J., Levin, I., Miller, J. B., et al.: Atmospheric radiocarbon for the period 1950–2019, Radiocarbon, 64, 723–745, 2022.

Hubau, W., Lewis, S. L., Phillips, O. L., Affum-Baffoe, K., Beeckman, H., Cuní-Sanchez, A., Daniels, A. K., Ewango, C. E., Fauset, S., Mukinzi, J. M., et al.: Asynchronous carbon sink saturation in African and Amazonian tropical forests, Nature, 579, 80–87, 2020.

Jung, M., Schwalm, C., Migliavacca, M., Walther, S., Camps-Valls, G., Koirala, S., Anthoni, P., Besnard, S., Bodesheim, P., Carvalhais, N., et al.: Scaling carbon fluxes from eddy covariance sites to globe: synthesis and evaluation of the FLUXCOM approach, Biogeosciences, 2020.

Keeling, C. D.: The concentration and isotopic abundances of atmospheric carbon dioxide in rural areas, Geochimica et cosmochimica acta, 13, 322–334, https://doi.org/10.1016/0016-7037(58)90033-4, 1958.

Keeling, C. D.: The concentration and isotopic abundances of carbon dioxide in rural and marine air, Geochimica et Cosmochimica Acta, 24, 277–298, https://doi.org/10.1016/0016-7037(61)90023-0, 1961.

Knohl, A., Werner, R. A., Brand, W. A., and Buchmann, N.: Short-term variations in δ 13 C of ecosystem respiration reveals link between assimilation and respiration in a deciduous forest, Oecologia, 142, 70–82, 2005.

Kromer, B. and Münnich, K. O.: CO_2 gas proportional counting in radiocarbon dating—review and perspective, Radiocarbon after four decades: An interdisciplinary perspective, pp. 184–197, 1992.

Levin, I., Münnich, K., and Weiss, W.: The effect of anthropogenic CO_2 and ^{14}C sources on the distribution of ^{14}C in the atmosphere, Radiocarbon, 22, 379–391, https://doi.org/10.1017/S003382220000967X, 1980.

Levin, I., Naegler, T., Kromer, B., Diehl, M., Francey, R., Gomez-Pelaez, A., Steele, P., Wagenbach, D., Weller, R., and Worthy, D.: Observations and modelling of the global distribution and long-term trend of atmospheric 14CO2, Tellus B: Chemical and Physical Meteorology, 62, 26–46, 2010.

Levin, I., Karstens, U., Eritt, M., Maier, F., Arnold, S., Rzesanke, D., Hammer, S., Ramonet, M., Vítková, G., Conil, S., et al.: A dedicated flask sampling strategy developed for Integrated Carbon Observation System (ICOS) stations based on CO 2 and CO measurements and Stochastic Time-Inverted Lagrangian Transport (STILT) footprint modelling, Atmospheric Chemistry and Physics, 20, 11 161–11 180, 2020.

Levin, I., Hammer, S., Kromer, B., Preunkert, S., Weller, R., and Worthy, D. E.: Radiocarbon in global tropospheric carbon dioxide, Radiocarbon, 64, 781–791, 2022.

Lu, X., Wang, Y.-P., Luo, Y., and Jiang, L.: Ecosystem carbon transit versus turnover times in response to climate warming and rising atmospheric CO_2 concentration, Biogeosciences, 15, 6559–6572, https://doi.org/10.5194/bg-15-6559-2018, 2018.

Lux, J. T.: A new target preparation facility for high precision AMS measurements and strategies for efficient $^{14}CO_2$ sampling, Ph.D. thesis, Faculty of Physics and Astronomy/Institute of Environmental Physics, https://doi.org/10.11588/heidok.00024767, 2018.

Malhi, Y., Baldocchi, D., and Jarvis, P.: The carbon balance of tropical, temperate and boreal forests, Plant, Cell & Environment, 22, 715–740, https://doi.org/10.1046/j.1365-3040.1999.00453.x, 1999.

Malhi, Y., Doughty, C., and Galbraith, D.: The allocation of ecosystem net primary productivity in tropical forests, Philosophical Transactions of the Royal Society B: Biological Sciences, 366, 3225–3245, 2011.

Malhi, Y., Doughty, C. E., Goldsmith, G. R., Metcalfe, D. B., Girardin, C. A. J., Marthews, T. R., del Aguila-Pasquel, J., Aragão, L. E. O. C., Araujo-Murakami, A., Brando, P., da Costa, A. C. L., Silva-Espejo, J. E., Farfán Amézquita, F., Galbraith, D. R., Quesada, C. A., Rocha, W., Salinas-Revilla, N., Silvério, D., Meir, P., and Phillips, O. L.: The linkages between photosynthesis, productivity, growth and biomass in lowland Amazonian forests, Global Change Biology, 21, 2283–2295, https://doi.org/10.1111/gcb.12859, 2015.

Marsh, E. J., Bruno, M. C., Fritz, S. C., Baker, P., Capriles, J. M., and Hastorf, C. A.: IntCal, SHCal, or a mixed curve? Choosing a 14C calibration curve for archaeological and paleoenvironmental records from tropical South America, Radiocarbon, 60, 925–940, 2018.

Mauritz, M., Celis, G., Ebert, C., Hutchings, J., Ledman, J., Natali, S., Pegoraro, E., Salmon, V., Schädel, C., Taylor, M., et al.: Using stable carbon isotopes of seasonal ecosystem respiration to determine permafrost carbon loss, Journal of Geophysical Research: Biogeosciences, 124, 46–60, 2019.

Metzler, H. and Sierra, C. A.: Linear autonomous compartmental models as continuous-time Markov chains: Transit-time and age distributions, Mathematical Geosciences, 50, 1–34, https://doi.org/10.1007/s11004-017-9690-1, 2018.

Miller, J. B. and Tans, P. P.: Calculating isotopic fractionation from atmospheric measurements at various scales, Tellus B: Chemical and Physical Meteorology, 55, 207–214, https://doi.org/10.3402/tellusb.v55i2.16697, 2003.

Miller, J. B., Lehman, S. J., Verhulst, K. R., Miller, C. E., Duren, R. M., Yadav, V., Newman, S., and Sloop, C. D.: Large and seasonally varying biospheric CO2 fluxes in the Los Angeles megacity revealed by atmospheric radiocarbon, Proceedings of the National Academy of Sciences, 117, 26 681–26 687, 2020.

Muñoz, E., Chanca, I., and Sierra, C. A.: Increased atmospheric CO2 and the transit time of carbon in terrestrial ecosystems, Global Change Biology, in press, https://doi.org/10.1111/gcb.16961, 2023.

Ometto, J. P., Flanagan, L. B., Martinelli, L. A., Moreira, M. Z., Higuchi, N., and Ehleringer, J. R.: Carbon isotope discrimination in forest and pasture ecosystems of the Amazon Basin, Brazil, Global Biogeochemical Cycles, 16, 56–1, 2002.

Pataki, D., Ehleringer, J., Flanagan, L., Yakir, D., Bowling, D., Still, C., Buchmann, N., Kaplan, J. O., and Berry, J.: The application and interpretation of Keeling plots in terrestrial carbon cycle research, Global biogeochemical cycles, 17, https://doi.org/10.1029/2001GB001850, 2003.

Phillips, C. L., McFarlane, K. J., LaFranchi, B., Desai, A. R., Miller, J. B., and Lehman, S. J.: Observations of $^{14}CO_2$ in ecosystem respiration from a temperate deciduous forest in Northern Wisconsin, Journal of Geophysical Research: Biogeosciences, 120, 600–616, https://doi.org/10.1002/2014JG002808, 2015.

Phillips, O. L. and Brienen, R. J.: Carbon uptake by mature Amazon forests has mitigated Amazon nations' carbon emissions, Carbon Balance and Management, 12, 1–9, 2017.

Pöhlker, C., Walter, D., Paulsen, H., Könemann, T., Rodríguez-Caballero, E., Moran-Zuloaga, D., Brito, J., Carbone, S., Degrendele, C., Després, V. R., et al.: Land cover and its transformation in the backward trajectory footprint region of the Amazon Tall Tower Observatory, Atmospheric Chemistry and Physics, 19, 8425–8470, 2019.

Rasmussen, M., Hastings, A., Smith, M. J., Agusto, F. B., Chen-Charpentier, B. M., Hoffman, F. M., Jiang, J., Todd-Brown, K. E., Wang, Y., Wang, Y.-P., et al.: Transit times and mean ages for nonautonomous and autonomous compartmental systems, Journal of mathematical biology, 73, 1379–1398, https://doi.org/10.1007/s00285-016-0990-8, 2016.

Reimer, P. J., Brown, T. A., and Reimer, R. W.: Discussion: reporting and calibration of post-bomb ^{14}C data, Radiocarbon, 46, 1299–1304, 2004.

Saturno, J., Holanda, B. A., Pöhlker, C., Ditas, F., Wang, Q., Moran-Zuloaga, D., Brito, J., Carbone, S., Cheng, Y., Chi, X., et al.: Black and brown carbon over central Amazonia: long-term aerosol measurements at the ATTO site, Atmospheric Chemistry and Physics, 18, 12 817–12 843, 2018.

Sedjo, R. and Sohngen, B.: Carbon sequestration in forests and soils, Annu. Rev. Resour. Econ., 4, 127–144, 2012.

Sierra, C. A., Harmon, M. E., Moreno, F. H., Orrego, S. A., and del Valle, J. I.: Spatial and temporal variability of net ecosystem production in a tropical forest: testing the hypothesis of a significant carbon sink, Global Change Biology, 13, 838–853, https://doi.org/10.1111/j.1365-2486.2007.01336.x, 2007.

Sierra, C. A., Müller, M., Metzler, H., Manzoni, S., and Trumbore, S. E.: The muddle of ages, turnover, transit, and residence times in the carbon cycle, Global change biology, 23, 1763–1773, https://doi.org/10.1111/gcb.13556, 2017.

Sierra, C. A., Crow, S. E., Heimann, M., Metzler, H., and Schulze, E.-D.: The climate benefit of carbon sequestration, Biogeosciences, 18, 1029–1048, https://doi.org/10.5194/bg-18-1029-2021, 2021a.

Sierra, C. A., Estupinan-Suarez, L. M., and Chanca, I.: The fate and transit time of carbon in a tropical forest, Journal of Ecology, https://doi.org/10.1111/1365-2745.13723, 2021b.

Sierra, C. A., Quetin, G. R., Metzler, H., and Müller, M.: A decrease in the age of respired carbon from the terrestrial biosphere and increase in the asymmetry of its distribution, Philosophical Transactions of the Royal Society A: Mathematical, Physical and Engineering Sciences, 381, 20220 200, https://doi.org/10.1098/rsta.2022.0200, 2023.

Stephens, B. B., Gurney, K. R., Tans, P. P., Sweeney, C., Peters, W., Bruhwiler, L., Ciais, P., Ramonet, M., Bousquet, P., Nakazawa, T., et al.: Weak northern and strong tropical land carbon uptake from vertical profiles of atmospheric CO_2, Science, 316, 1732–1735, https://doi.org/10.1126/science.1137004, 2007.

Steur, P. M., Botter, D., Scheeren, H. A., Moossen, H., Rothe, M., and Meijer, H. A.: Preventing drift of oxygen isotopes of CO_2-in-air stored in glass sample flasks: new insights and recommendations, Isotopes in Environmental and Health Studies, 59, 309–326, 2023.

Stuiver, M. and Polach, H. A.: Discussion reporting of ^{14}C data, Radiocarbon, 19, 355–363, https://doi.org/10.1017/S0033822200003672, 1977.

Tans, P. P.: On calculating the transfer of carbon-13 in reservoir models of the carbon cycle, Tellus, 32, 464–469, 1980.

Telles, E. d. C. C., de Camargo, P. B., Martinelli, L. A., Trumbore, S. E., da Costa, E. S., Santos, J., Higuchi, N., and Oliveira Jr, R. C.: Influence of soil texture on carbon dynamics and storage potential in tropical forest soils of Amazonia, Global Biogeochemical Cycles, 17, https://doi.org/10.1029/2002GB001953, 2003.

Thoning, K. W., Tans, P. P., and Komhyr, W. D.: Atmospheric carbon dioxide at Mauna Loa Observatory: 2. Analysis of the NOAA GMCC data, 1974–1985, Journal of Geophysical Research: Atmospheres, 94, 8549–8565, 1989.

Trumbore, S.: Carbon respired by terrestrial ecosystems – recent progress and challenges, Global Change Biology, 12, 141–153, https://doi.org/10.1111/j.1365-2486.2006.01067.x, 2006.

Trumbore, S. and De Camargo, P. B.: Soil carbon dynamics, Amazonia and global change, 186, 451–462, https://doi.org/10.1029/2008GM000741, 2009.

Trumbore, S., Da Costa, E. S., Nepstad, D. C., Barbosa De Camargo, P., Martinelli, L. A., Ray, D., Restom, T., and Silver, W.: Dynamics of fine root carbon in Amazonian tropical ecosystems and the contribution of roots to soil respiration, Global Change Biology, 12, 217–229, https://doi.org/10.1111/j.1365-2486.2005.001063.x, 2006.

Turnbull, J. C., Mikaloff Fletcher, S. E., Brailsford, G. W., Moss, R. C., Norris, M. W., and Steinkamp, K.: Sixty years of radiocarbon dioxide measurements at Wellington, New Zealand: 1954–2014, Atmospheric Chemistry and Physics, 17, 14 771–14 784, 2017.

Vieira, S., Trumbore, S., Camargo, P. B., Selhorst, D., Chambers, J. Q., Higuchi, N., and Martinelli, L. A.: Slow growth rates of Amazonian trees: consequences for carbon cycling, Proceedings of the National Academy of Sciences, 102, 18 502–18 507, https://doi.org/10.1073/pnas.0505966102, 2005.

Wendeberg, M., Richter, J., Rothe, M., and Brand, W. A.: Jena Reference Air Set (JRAS): a multi-point scale anchor for isotope measurements of CO 2 in air, Atmospheric Measurement Techniques, 6, 817–822, 2013.

Zobitz, J., Keener, J., Schnyder, H., and Bowling, D.: Sensitivity analysis and quantification of uncertainty for isotopic mixing relationships in carbon cycle research, Agricultural and Forest Meteorology, 136, 56–75, 2006.